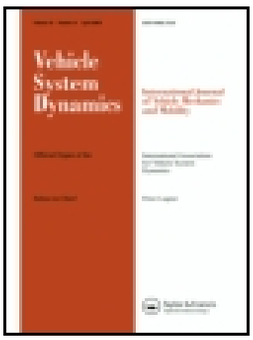

Vehicle System Dynamics

ISSN: 0042-3114 (Print) 1744-5159 (Online) Journal homepage: https://www.tandfonline.com/loi/nvsd20

# Real-time models for wheels and tyres in an object-oriented modelling framework

Dirk Zimmer & Martin Otter

**To cite this article:** Dirk Zimmer & Martin Otter (2010) Real-time models for wheels and tyres in an object-oriented modelling framework, Vehicle System Dynamics, 48:2, 189-216, DOI: 10.1080/00423110802687596

**To link to this article:** https://doi.org/10.1080/00423110802687596

*Vehicle System Dynamics*
Vol. 48, No. 2, February 2010, 189–216

Taylor & Francis
Taylor & Francis Group

# Real-time models for wheels and tyres in an object-oriented modelling framework

Dirk Zimmer[a]* and Martin Otter[b]

[a]*Department of Computer Science, Institute of Computational Science, ETH Zürich, Switzerland;*
[b]*Institut für Robotik und Mechatronik, Deutsches Zentrum für Luft- und Raumfahrt e.V., Wessling, Germany*

(*Received 21 May 2008; final version received 11 December 2008; first published 5 March 2009*)

This article presents models for wheels and tyres in the application field of real-time multi-body systems. For this rather broad class of applications it is difficult to foresee the right level of model complexity that is affordable in a specific simulation. Therefore we developed a tyre model that is adjustable in its degree of complexity. It consists of a list of stepwise developed sub-models, each at a higher level of complexity. These models include semi-empirical equations. The stepwise development process is also reflected in the corresponding implementation with the modelling language Modelica. The final wheel model represents a supermodel and enables users to select the right level of complexity in an unambiguous way.

**Keywords:** tyre models; multi-body dynamics; object-oriented modelling; Modelica

## 1. Introduction

This article presents a set of successively constructed models for wheels and tyres. These models have been primarily designed for their application in real-time simulations of multi-body systems. Hence they are based upon fundamental mechanical laws and are then further extended by a number of empirical formulas. The set of models forms a list where each further model in the list is built on its predecessors and adds more detail and complexity. The final model represents an elaborated semi-empirical tyre model that defines about 200 scalar equations.

A number of semi-empirical tyre models have been designed during the last decades and form the basis of our approach. The most known of them is the Magic-Formula model of Pacejka [1]. Another important one, especially for real-time applications, is the TMeasy model and its predecessors from [2–4]. The latter model is the basis of this article and is improved in various directions. Further important contributions in the field of semi-empirical tyre models

*Corresponding author. Email: dzimmer@inf.ethz.ch

ISSN 0042-3114 print/ISSN 1744-5159 online

DOI: 10.1080/00423110802687596
http://www.informaworld.com

were made by Schmeitz [5], Gipser [6] and Svendenius and Gäfvert [7]. Other contributions have been made by Gim *et al*. [8] and Guo and Lu [9].

The focus in the field of modelling and simulation is nowadays shifting from the pure computational tasks towards the organisation of knowledge. Modern modelling languages such as Modelica [10] and their corresponding simulation environments enable an open and object-oriented modelling approach and are becoming increasingly prevalent. The integration of tyre models into a general object-oriented modelling methodology is therefore of major importance.

To this end, we have implemented our models in Modelica and integrated interfaces to existing MultiBody [11] and vehicle-systems libraries [12]. The object-oriented mechanisms of this language enable us to take a stepwise approach that consists of a sequence of models. The first model of this sequence represents the simple model of an ideal rolling wheel. Starting from here each new model introduces a new level of complexity. Effects of friction, slip and tyre deformation are successively taken into account. In total, seven models have been generated. The first three levels of complexity are built upon fundamental laws, known friction laws and idealisations. From level 4 on, empirical formulas are included in the model that are based on the tyre model of Rill [4] together with improvements and enhancements.

The stepwise modelling features important advantages: since the corresponding implementation provides a uniform interface for all models, the user can alternate between the different variants in an unambiguous way. The most suitable level of complexity can therefore be determined conveniently and practically. The highest levels are not necessarily the best selection for real-time simulations: these models have a higher computational effort and demand more precise model knowledge. In contrast, simpler models are less demanding concerning both computational effort and data identification.

The stepwise evolvement of complexity also helps to avoid difficulties in understanding. The process of modelling becomes more transparent and a study of the internal equations becomes a feasible task. This is an important prerequisite to add further features into the models. In contrast to developers, an ordinary user may prefer a more empirical approach. He can then study step by step all the successively added aspects by means of provided experimental setups. This represents an easy way to achieve an intuitive understanding of the model behaviour.

The tyre models of this article are designed to be used for vehicles, motorcycles and bicycles. Hence a number of important aspects had to be regarded during the development. The wheel models are not restricted to certain specific driving situations. Most of the relevant cases have been considered. In some borderline cases, the model behaviour may be inaccurate but at least good natured. The set of specification parameters has been selected to provide a good trade-off between generality and accuracy. The models can be used as a starting point for further specialisation, concerning, e.g. bicycle wheels as well as truck wheels. The complexity of the model does not exceed the limit that is needed for a real-time simulation. Even more complex systems should be integrable in real time on a usual contemporary machine.

## 2. Fundamental geometrical properties

This section introduces the used notation and the underlying geometric assumptions. The notation of all algebraic variables and parameters obeys the following rules: symbols that represent vectors or matrices are printed in bold face. Vectors are resolved with respect to their corresponding body system (here: the wheel's system), if not stated otherwise. The appearance of '0' in the lower index denotes that the vector is resolved with respect to the inertial system. The correspondence of a scalar to a vector's direction is also represented by a lower index.

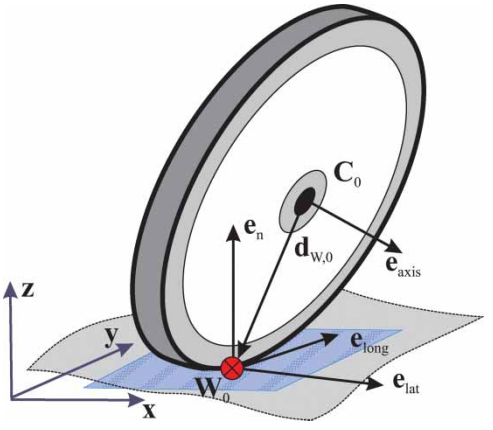


Figure 1. Fundamental geometrical properties.

For example, the scalar $f_{\text{lat}}$ denotes the force in lateral direction that is given by $\boldsymbol{e}_{\text{lat}}$. All unit vectors are denoted by an $\boldsymbol{e}$ and are resolved in the inertial system if not stated otherwise. Please note that Appendix 1 provides a comprehensive overview of notation used in this article.

Figure 1 introduces the fundamental geometric variables. The road is a surface in three-dimensional space. It is locally approximated by its tangent plane which is defined by its normal vector $\boldsymbol{e}_{\text{n}}$. The absolute position of the centre of the wheel is denoted by vector $\boldsymbol{C}_0$. The rotation axis of the wheel is described by the unit vector $\boldsymbol{e}_{\text{axis}}$, that also represents the $y$-vector of the wheel's body system. The contact between wheel and road is preliminarily assumed to be determined by a single point. While this assumption is sufficient and reasonable for rigid wheels it definitely does not hold for deformable components like a tyre where the contact is defined by a complex area instead of a single point. However, the concept of a contact point remains meaningful, since it can be applied to represent the contact area in an approximative way, by the introduction of the penetration depth along the road normal.

The absolute position of the contact point is given by $\boldsymbol{W}_0$. It is always located on the undeformed wheel shape. The distance vector between wheel centre and contact point is denoted by $\boldsymbol{d}_{\text{W},0}$. The vectors $\boldsymbol{e}_{\text{n}}$, $\boldsymbol{e}_{\text{lat}}$ and $\boldsymbol{e}_{\text{long}}$ span a coordinate system at the point of contact. The lateral direction $\boldsymbol{e}_{\text{lat}}$ is defined by the projection of $\boldsymbol{e}_{\text{axis}}$ on the road plane and the longitudinal direction $\boldsymbol{e}_{\text{long}}$ is perpendicular to both $\boldsymbol{e}_{\text{lat}}$ and $\boldsymbol{e}_{\text{n}}$:

$$\boldsymbol{e}_{\text{long}} = \text{normalise}(\boldsymbol{e}_{\text{n}} \times \boldsymbol{e}_{\text{axis}}), \tag{1}$$

$$\boldsymbol{e}_{\text{lat}} = \boldsymbol{e}_{\text{long}} \times \boldsymbol{e}_{\text{n}} \tag{2}$$

with function $\text{normalise}(x) = x/|x|$. The contact point $\boldsymbol{W}_0$ is determined by the positional state $(\boldsymbol{C}_0, \boldsymbol{e}_{\text{axis}})$ and the geometry of wheel and road. The interface for the road geometry is provided in a general way. The road is modelled as a surface that is described in parameterised form by two surface parameters $s$ (=usually along the road heading direction) and $w$ (=usually along the lateral direction of the road). Properties of the road can be inquired by function calls [13], most important:

$$\boldsymbol{r}_{\text{road},0} = \text{roadPosition}(s, w), \tag{3}$$

$$\boldsymbol{e}_{\text{n}} = \frac{\partial \boldsymbol{r}_{\text{road},0}}{\partial s} \times \frac{\partial \boldsymbol{r}_{\text{road},0}}{\partial w} = \text{roadNormal}(s, w), \tag{4}$$

$$\boldsymbol{e}_{\text{s}} = \frac{\partial \boldsymbol{r}_{\text{road},0}}{\partial s} = \text{roadHeading}(s, w), \tag{5}$$

where roadPosition( . . . ) returns the absolute position vector to a point on the road defined by the surface parameters $(s,w)$, roadNormal( . . . ) returns the road normal and roadHeading( . . . ) returns the heading direction (tangent along $s$) at this point. These functions can be, e.g. constructed from standard road segments (straight line, circle segment, clothoid), or from CAD data of a terrain model. In the latter case usually no road heading and lateral direction is defined and therefore $s$ and $w$ may then be selected to be the $x$ and $y$ axes of a road specific coordinate system. In both cases it is usually easy to select $s,w$ such that they represent the path length, i.e. $|\partial \boldsymbol{r}_{\text{road},0}/\partial s| = |\partial \boldsymbol{r}_{\text{road},0}/\partial w| = 1$. This simplifies the interpretation of $s,w$ as well as the contact computation.

The wheel geometry is defined by a closed surface. Currently, our implementation supports three different shapes: a flat disc, a torus and a voluminous wheel (=a torus truncated on two sides by planes). Figure 2 depicts the geometry of these three wheel shapes and presents their visualisation in the simulation environment. The choice of the wheel's shape influences essentially the lateral position and size of the contact patch and its corresponding pressure peak. For the contact point calculation, a function of form of Equation (6) has to be provided for every wheel shape to compute $\boldsymbol{d}_{\text{W},0}$, the distance vector between wheel centre and contact point. Table 1 summarises the resulting equations for the shapes of Figure 2. To this end, we define $\boldsymbol{e}_{\text{plane}}$ as an auxiliary variable. It represents a normalised projection of $\boldsymbol{e}_{\text{n}}$ on the imaginary wheel plane and is determined in Equation (7).

$$\boldsymbol{d}_{\text{W},0} = \text{distanceVector}(\boldsymbol{e}_{\text{n}}, \boldsymbol{e}_{\text{axis}}, \langle \text{shape parameters} \rangle), \tag{6}$$

$$\boldsymbol{e}_{\text{plane}} = \boldsymbol{e}_{\text{long}} \times \boldsymbol{e}_{\text{axis}}. \tag{7}$$

The contact point calculation includes two approaches: for level 1 (Section 3) and level 2 (Section 4) the geometric constraint is used that the (rigid) road and the (rigid) wheel surfaces must touch each other. For all other levels, no geometric constraint is present and the contact point is defined as the point on the (rigid) wheel surface that has the largest penetration depth.

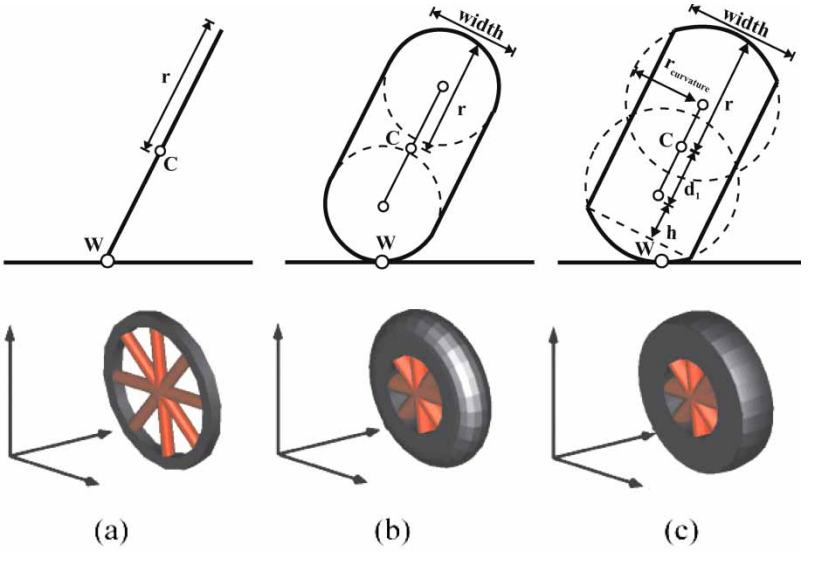


Figure 2. Three different wheel shapes: (a) flat disc, (b) torus and (c) voluminous wheel.

Table 1. Distance vectors for wheel shapes.

| | |
|---|---|
| Flat disc | $\boldsymbol{d}_{\mathrm{W},0} = -r \cdot \boldsymbol{e}_{\mathrm{plane}}$ |
| Torus | $\boldsymbol{d}_{\mathrm{W},0} = \left(\frac{\mathrm{width}}{2} - r\right) \cdot \boldsymbol{e}_{\mathrm{plane}} - \frac{\mathrm{width}}{2} \cdot \boldsymbol{e}_{\mathrm{n}}$ |
| Voluminous wheel | $\boldsymbol{d}_{\mathrm{W},0} = d_1 \cdot \boldsymbol{e}_{\mathrm{plane}} - d_2$ |
| | $d_1 = (r_{\mathrm{curvature}} - r)$ |
| | $d_2 = \begin{cases} -\boldsymbol{e}_{\mathrm{n}} \cdot r_{\mathrm{curvature}} & \text{if } \lvert\boldsymbol{e}_{\mathrm{axis}} \cdot \boldsymbol{e}_{\mathrm{n}}\rvert \le \frac{\mathrm{width}}{2r_{\mathrm{curvature}}} \\ \pm\boldsymbol{e}_{\mathrm{axis}} \cdot \frac{\mathrm{width}}{2} + h\frac{d_1}{\lvert d_1\rvert} & \text{if } \lvert\boldsymbol{e}_{\mathrm{axis}} \cdot \boldsymbol{e}_{\mathrm{n}}\rvert > \frac{\mathrm{width}}{2r_{\mathrm{curvature}}} \end{cases}$ |
| | $h = r_{\mathrm{curvature}} \cdot \sqrt{1 - \left(\frac{\mathrm{width}}{2r_{\mathrm{curvature}}}\right)^2}$ |

In both cases, the contact point calculation is described by the following equations:

$$\begin{aligned} \boldsymbol{r}_{\mathrm{road},0} &= \mathrm{roadPosition}(s, w), \\ \boldsymbol{e}_{\mathrm{n}} &= \mathrm{roadNormal}(s, w), \\ \boldsymbol{e}_{\mathrm{s}} &= \mathrm{roadHeading}(s, w), \\ \boldsymbol{e}_{\mathrm{w}} &= \boldsymbol{e}_{\mathrm{n}} \times \boldsymbol{e}_{\mathrm{s}}, \\ \boldsymbol{e}_{\mathrm{long}} &= \mathrm{normalise}(\boldsymbol{e}_{\mathrm{n}} \times \boldsymbol{e}_{\mathrm{axis}}), \\ \boldsymbol{e}_{\mathrm{plane}} &= \boldsymbol{e}_{\mathrm{long}} \times \boldsymbol{e}_{\mathrm{axis}} \end{aligned} \tag{8}$$

and additionally the following equations for a flat disc:

$$\begin{aligned} \boldsymbol{\delta} &= \boldsymbol{r}_{\mathrm{road},0} - \boldsymbol{C}_0, \\ 0 &= \boldsymbol{e}_{\mathrm{axis}} \cdot \boldsymbol{\delta} \quad \text{(residue 1 of algebraic equation system)}, \\ 0 &= \boldsymbol{e}_{\mathrm{long}} \cdot \boldsymbol{\delta} \quad \text{(residue 2 of algebraic equation system)}, \\ s_{\mathrm{n}} &= r - \boldsymbol{\delta} \cdot \boldsymbol{e}_{\mathrm{plane}} \quad \text{(penetration depth, or residue for rolling with } s_{\mathrm{n}} = 0) \end{aligned} \tag{9}$$

and the subsequent equations for the other wheel shapes:

$$\begin{aligned} \boldsymbol{d}_{\mathrm{W},0} &= \mathrm{distanceVector}(\boldsymbol{e}_{\mathrm{n}}, \boldsymbol{e}_{\mathrm{axis}}, \boldsymbol{e}_{\mathrm{plane}}, \langle\text{shape parameters}\rangle), \\ \boldsymbol{\delta} &= \boldsymbol{r}_{\mathrm{road},0} - \boldsymbol{C}_0 - \boldsymbol{d}_{\mathrm{W},0}, \\ 0 &= \boldsymbol{e}_{\mathrm{s}} \cdot \boldsymbol{\delta} \quad \text{(residue 1 of algebraic equation system)}, \\ 0 &= \boldsymbol{e}_{\mathrm{w}} \cdot \boldsymbol{\delta} \quad \text{(residue 2 of algebraic equation system)}, \\ s_{\mathrm{n}} &= \boldsymbol{e}_{\mathrm{n}} \cdot \boldsymbol{\delta} \quad \text{(penetration depth, or residue for rolling with } s_{\mathrm{n}} = 0). \end{aligned} \tag{10}$$

These equations assume that the wheel states ($\boldsymbol{C}_0$, $\boldsymbol{e}_{\mathrm{axis}}$) are known (e.g. computed from the states of the wheel and/or the vehicle) and that the two road parameters ($s$,$w$) are iteration variables of a nonlinear algebraic equation system with two equations: all left-hand side variables of Equations (8)–(10) can be computed from $\boldsymbol{C}_0$, $\boldsymbol{e}_{\mathrm{axis}}$, $s$,$w$. The second and third equations of Equations (9) and (10) are the residue equations of the algebraic equation system.

In the latter case it is defined that the road normal is perpendicular to the tangents of the wheel at the wheel contact point. The last equation computes the penetration depth $s_n$. For ideal rolling or slipping, this is an additional residue equation and then one (previous) state of the wheel or of the vehicle is additionally constraint and is computed from this residue equation.

Depending on the situation, derivatives of Equations (8)–(10) are needed, e.g. for describing ideal rolling. Modern M&S-environments detect such cases automatically and process a symbolic differentiation.

If the computing time to calculate the contact point must have a guaranteed upper limit (e.g. in the case of real-time simulations), the termination condition of the iterative nonlinear algebraic equation solver must be adapted, e.g. by terminating the solver after a maximum number of iterations. For the contact calculation above, this can be achieved by approximating the road description with a first-order Taylor series approximation around the contact point $s_{\text{last}}$,$w_{\text{last}}$ determined in the last integration step:

$$\begin{aligned}
\boldsymbol{r}_{\text{road},0} &\approx \text{roadPosition}(s_{\text{last}}, w_{\text{last}}) + \frac{\partial \boldsymbol{r}_{\text{road},0}}{\partial s}\Delta s + \frac{\partial \boldsymbol{r}_{\text{road},0}}{\partial w}\Delta w \\
&= \text{roadPosition}(s_{\text{last}}, w_{\text{last}}) + \boldsymbol{e}_s(s_{\text{last}}, w_{\text{last}})\Delta s + \boldsymbol{e}_w(s_{\text{last}}, w_{\text{last}})\Delta w, \qquad (11)\\
s &= s_{\text{last}} + \Delta s,\\
w &= w_{\text{last}} + \Delta w,
\end{aligned}$$

computing the partial derivatives of the road from the last calculated point:

$$\begin{aligned}
\boldsymbol{r}_{\text{road},0,\text{last}} &= \text{roadPosition}(s_{\text{last}}, w_{\text{last}}),\\
\boldsymbol{e}_{\text{n,last}} &= \text{roadNormal}(s_{\text{last}}, w_{\text{last}}),\\
\boldsymbol{e}_{\text{s,last}} &= \text{roadHeading}(s_{\text{last}}, w_{\text{last}}), \qquad (12)\\
\boldsymbol{e}_{\text{w,last}} &= \boldsymbol{e}_{\text{n,last}} \times \boldsymbol{e}_{\text{s,last}},\\
\boldsymbol{e}_{\text{long,last}} &= \text{normalise}(\boldsymbol{e}_{\text{n,last}} \times \boldsymbol{e}_{\text{axis}}),\\
\boldsymbol{e}_{\text{plane,last}} &= \boldsymbol{e}_{\text{long,last}} \times \boldsymbol{e}_{\text{axis}},
\end{aligned}$$

inserting the result in Equations (9) and (10) and simplifying the equations yielding for the flat disc the direct (non-iterative) solution:

$$\begin{aligned}
&\begin{bmatrix} \boldsymbol{e}_{\text{axis}} \cdot \boldsymbol{e}_{\text{s,last}} & \boldsymbol{e}_{\text{axis}} \cdot \boldsymbol{e}_{\text{w,last}} \\ \boldsymbol{e}_{\text{long,last}} \cdot \boldsymbol{e}_{\text{s,last}} & \boldsymbol{e}_{\text{long,last}} \cdot \boldsymbol{e}_{\text{w,last}} \end{bmatrix} \begin{bmatrix} \Delta s \\ \Delta w \end{bmatrix} = \begin{bmatrix} \boldsymbol{e}_{\text{axis}} \cdot (\boldsymbol{C}_0 - \boldsymbol{r}_{\text{road},0,\text{last}}) \\ \boldsymbol{e}_{\text{long,last}} \cdot (\boldsymbol{C}_0 - \boldsymbol{r}_{\text{road},0,\text{last}}) \end{bmatrix},\\
&\boldsymbol{r}_{\text{road},0,\text{last}} + \boldsymbol{e}_{\text{s,last}}\Delta s + \boldsymbol{e}_{\text{w,last}}\Delta w - \boldsymbol{C}_0 = \boldsymbol{\delta},\\
&r - \boldsymbol{\delta} \cdot \boldsymbol{e}_{\text{plane,last}} = s_{\text{n}} \qquad (13)
\end{aligned}$$

and for the other wheel shapes correspondingly:

$$\begin{aligned}
\boldsymbol{d}_{\text{W},0,\text{last}} &= \text{distanceVector}(\boldsymbol{e}_{\text{n,last}}, \boldsymbol{e}_{\text{axis}}, \boldsymbol{e}_{\text{plane,last}}, \langle\text{shape parameters}\rangle),\\
\boldsymbol{\delta}_{\text{last}} &= \boldsymbol{r}_{\text{road},0,\text{last}} - \boldsymbol{C}_0 - \boldsymbol{d}_{\text{W},0,\text{last}},\\
\Delta s &= -\boldsymbol{e}_{\text{s,last}} \cdot \boldsymbol{\delta}_{\text{last}}, \qquad (14)\\
\Delta w &= -\boldsymbol{e}_{\text{w,last}} \cdot \boldsymbol{\delta}_{\text{last}},\\
s_{\text{n}} &= \boldsymbol{e}_{\text{n,last}} \cdot (\boldsymbol{\delta}_{\text{last}} + \boldsymbol{e}_{\text{s,last}}\Delta s + \boldsymbol{e}_{\text{w,last}}\Delta w).
\end{aligned}$$

In order to improve the precision of the contact point calculation, Equations (11)–(14) can be evaluated several times.

## 3. Ideal rolling wheels (level 1)

This paragraph introduces briefly the fundamental equations of motion and their corresponding variables and parameters. The wheel's inertia is defined by its mass $m$ and its inertia tensor $\boldsymbol{I}$. The translational position and motion of the wheel are described with respect to the inertial system by the position $\boldsymbol{C}_0$ and the velocity $\boldsymbol{v}_0$. The orientation of the wheel is described by the rotational matrix $\boldsymbol{R}$, where the columns of $\boldsymbol{R}$ represent the unit vectors of the body system resolved in the inertial frame. The translational and angular momentum equations are both resolved in the body fixed frame, since the computation is most efficient here. Therefore inertia tensor, angular velocity $\boldsymbol{\omega}$, as well as the resultant force $\boldsymbol{f}$ and torque $\boldsymbol{t}$ at the centre of mass are resolved in the body fixed frame. The gravity acceleration $\boldsymbol{g}_0$ acts on the centre point of the wheel whereas the force $\boldsymbol{f}_{\text{tyre},0}$ represents the force that acts on the contact point of the wheel. The equations of motion are stated in the presented notation as:

$$\boldsymbol{v}_0 = \dot{\boldsymbol{C}}_0, \tag{15}$$

$$\boldsymbol{f} = \boldsymbol{R}\left(m \cdot \dot{\boldsymbol{v}}_0 - m \cdot \boldsymbol{g}_0 - \boldsymbol{f}_{\text{tyre},0}\right), \tag{16}$$

$$\boldsymbol{\omega} = \begin{bmatrix} \boldsymbol{R}_3^{\mathrm{T}} \cdot \dot{\boldsymbol{R}}_2 \\ -\boldsymbol{R}_3^{\mathrm{T}} \cdot \dot{\boldsymbol{R}}_1 \\ \boldsymbol{R}_2^{\mathrm{T}} \cdot \dot{\boldsymbol{R}}_1 \end{bmatrix} \quad \text{with } \boldsymbol{R} = [\boldsymbol{R}_1, \ \boldsymbol{R}_2, \ \boldsymbol{R}_3], \tag{17}$$

$$\boldsymbol{t} = \boldsymbol{I}\dot{\boldsymbol{\omega}} + \boldsymbol{\omega} \times \boldsymbol{I}\boldsymbol{\omega} + \boldsymbol{R}(\boldsymbol{d}_{\text{W},0} \times \boldsymbol{f}_{\text{tyre},0}). \tag{18}$$

For a rigid wheel the contact between the wheel and the (rigid) road leads to a holonomic constraint, as described by Equation (8) with $s_{\text{n}} = 0$.

The slip velocity is defined to be the velocity difference between the contact point and the road. Based on the reasonable assumption that the ground is not moving, the slip velocity equals the velocity at the contact-point. It can be decomposed into a lateral and a longitudinal component:

$$v\text{Slip}_{\text{lat}} = (\boldsymbol{v}_0 + \boldsymbol{\omega}_0 \times \boldsymbol{d}_{\text{W},0})) \cdot \boldsymbol{e}_{\text{lat}}, \tag{19}$$

$$v\text{Slip}_{\text{long}} = (\boldsymbol{v}_0 + \boldsymbol{\omega}_0 \times \boldsymbol{d}_{\text{W},0})) \cdot \boldsymbol{e}_{\text{long}}, \tag{20}$$

$$\boldsymbol{\omega}_0 = \boldsymbol{R}^{\mathrm{T}}\boldsymbol{\omega}. \tag{21}$$

Ideal rolling is defined by the property that the slip velocity is zero, i.e. there is no slippage. Thus, two non-holonomic constraints are introduced:

$$v\text{Slip}_{\text{lat}} = 0, \tag{22}$$

$$v\text{Slip}_{\text{long}} = 0. \tag{23}$$

The force $\boldsymbol{f}_{\text{tyre},0}$ is composed out of the lateral, longitudinal and normal components: $f_{\text{lat}}$, $f_{\text{long}}$ and $f_{\text{n}}$ that uphold their corresponding constraint equations.

$$\boldsymbol{f}_{\text{tyre},0} = \boldsymbol{e}_{\text{n}} f_{\text{n}} + \boldsymbol{e}_{\text{lat}} f_{\text{lat}} + \boldsymbol{e}_{\text{long}} f_{\text{long}}. \tag{24}$$

For an ideal rolling wheel there remain five degrees of freedom on positional level and three degrees of freedom on the level of velocity. Hence the resulting model contains eight state variables. In case of a flat road, the holonomic contact equations (8) are linear and no longer nonlinear: if the wheel is situated on its own or attached to an elastic suspension model, only small-sized linear equation systems have to be solved during integration. However, a

nonlinear equation system may result out of the non-penetration condition if wheels are rigidly connected. For instance, a model of an ideal rolling, rigid bicycle contains a single bi-quadratic equation.

## 4. Rigid wheel with slip (level 2)

To arrive at a more realistic tyre model, the ideal rolling condition is abandoned by modelling the slippage. This is performed by removing the two non-holonomic constraint equations (22) and (23). The former constraint forces $f_{\text{lat}}$ and $f_{\text{long}}$ are now calculated as function of the total slip velocity $v\text{Slip}$. According to Coulombs's law for dry friction, the friction force counteracts the slip velocity and is proportional to the normal load $f_{\text{n}}$ and the friction coefficient $\mu_{v\text{Slip}}$. The friction coefficient $\mu_{v\text{Slip}}$ itself can be interpreted to be dependent on the total slip velocity $v\text{Slip}$. This dependency is shown by the solid line in Figure 3.

$$f_{\text{lat}} = -f_{\text{n}}\mu_{v\text{Slip}}\frac{v\text{Slip}_{\text{lat}}}{v\text{Slip}}, \tag{25}$$

$$f_{\text{long}} = -f_{\text{n}}\mu_{v\text{Slip}}\frac{v\text{Slip}_{\text{long}}}{v\text{Slip}}, \tag{26}$$

$$v\text{Slip} = \left|v\text{Slip}_{\text{lat}}\boldsymbol{e}_{\text{lat}} + v\text{Slip}_{\text{long}}\boldsymbol{e}_{\text{long}}\right| = \left|\boldsymbol{v}_0 + \boldsymbol{\omega}_0 \times \boldsymbol{d}_{\text{W},0}\right|. \tag{27}$$

This dependency models the transition from stiction to (sliding) friction. The latter case is given if the slip velocity exceeds a certain threshold $v\text{Slide}$. The friction coefficient $\mu_{v\text{Slip}}$ is then represented by a constant value $\mu_{\text{min}}$ . For lower slip velocities the friction coefficient increases continuously up to value $\mu_{\text{max}}$, that represents the point of maximum possible force

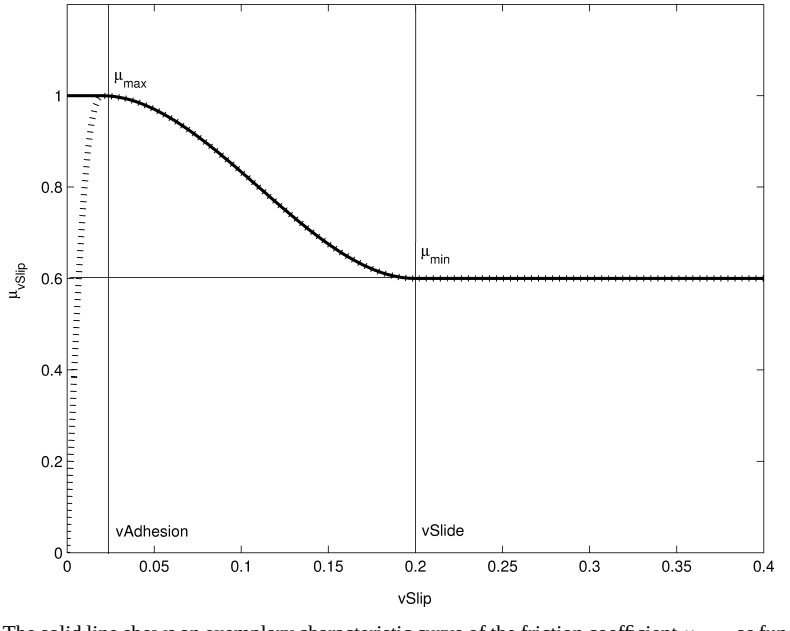


Figure 3. The solid line shows an exemplary characteristic curve of the friction coefficient $\mu_{v\text{Slip}}$ as function of the slip velocity. The dotted line represents the corresponding regularisation to avoid the ideal rolling phase or alternatively the high stiffness in case of rest.

transmission in case of stiction. Stiction at the contact point represents ideal rolling. At this point, a division by zero occurs in the above equations.

This transition from rolling with slippage to ideal rolling is a critical issue since Equations (25) and (26) become a potential source of stiffness for low slip velocities: minor changes of the slip velocity may lead to a drastic change of the resulting friction force. Thus, the slip velocity is unlikely to become zero just by the process of integration. Furthermore a proper modelling of the transition would include the introduction of two non-holonomic constraints. This implies a significant change of the model structure (e.g. state selection) during simulation time, that still represents an infeasible task for many of the current simulation systems.

A possible attempt to overcome these problems is the usage of a regularised characteristic at small slip velocities. To this end, a range of adhesion is artificially introduced into the model. Its boundary value $v\text{Adhesion}$ is set to a small arbitrary value, e.g. 1 mm/s. Within this range of adhesion the two non-holonomic constraints are formulated in a relaxed way as function of the slip velocity so that the corresponding curve crosses the origin. In consequence, the original stiffness of the model has been reduced. The regularised curve is represented by the dotted line in Figure 3.

This curve is determined by a continuous interpolation between the characteristic points ($v\text{Adhesion}$, $\mu_{\max}$) and ($v\text{Slide}$, $\mu_{\min}$). This piecewise polynomial equation ensures that the first derivative is well defined at all points of the curve. This interpolation scheme has already been used by Rill [4]. It will be further applied in subsequent sections.

$$\mu_{v\text{Slip}} = \begin{cases} \dfrac{v\text{Slip} \cdot \dot{\mu}_{v\text{Slip}}(0)}{1 + \sigma((v\text{Adhesion}/\mu_{\max})\dot{\mu}_{v\text{Slip}}(0) - 2 + \sigma)} & \text{if } v\text{Slip} \le v\text{Adhesion}, \\ & \sigma = \dfrac{v\text{Slip}}{v\text{Adhesion}}, \\ \mu_{\max} - (\mu_{\max} - \mu_{\min})\sigma^2(3 - 2\sigma) & \text{if } v\text{Adhesion} < v\text{Slip} < v\text{Slide}, \\ & \sigma = \dfrac{v\text{Slip} - v\text{Adhesion}}{v\text{Slide} - v\text{Adhesion}}, \\ \mu_{\min} & \text{else.} \end{cases} \tag{28}$$

This regularisation ensures that the fraction $\mu_{v\text{Slip}}/v\text{Slip}$ is now always properly defined, since it can be reduced by the term $v\text{Slip}$ for small slip velocities ($v\text{Slip} < v\text{Adhesion}$). To avoid any potential problems due to a division by zero, the term $\mu_{v\text{Slip}}/v\text{Slip}$ is symbolically resolved and Equations (25) and (26) are modified correspondingly. The new form avoids numerical difficulties:

$$f_{\text{lat}} = f_{\text{n}} \left( \frac{\mu_{v\text{Slip}}}{v\text{Slip}} \right) v\text{Slip}_{\text{lat}}, \tag{29}$$

$$f_{\text{long}} = f_{\text{n}} \left( \frac{\mu_{v\text{Slip}}}{v\text{Slip}} \right) v\text{Slip}_{\text{long}}. \tag{30}$$

The resulting model contains 10 state variables: five pairs of positional and velocity variables. Two algebraic equation systems have to be solved for integration, one of them is always linear. As in the previous model, the holonomic constraint may lead to a nonlinear equation system in case the road is not a plane and/or the wheel is rigidly suspended. The major drawback that is naturally associated with the regularisation results from the tolerance of slight errors within the range of adhesion. In static cases (e.g. an uphill parked car) the slight error might integrate over time and the solution becomes insufficient. However, these cases do not represent the field of interest of these tyre models.

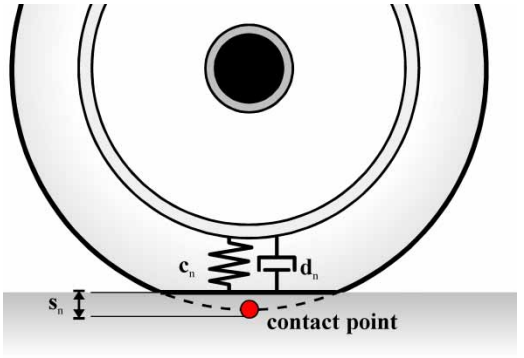


Figure 4. The deformation of the tyre in direction of the road normal is modelled by a virtual spring–damper element.

## 5. Wheels with simple slick tyre (level 3)

The model of a rigid wheel is extended to a simple elastic tyre model. Such a wheel is no longer holonomically constrained and therefore owns by itself six degrees of freedom. The tyre is modelled by a virtual spring–damper system as sketched in Figure 4. Since wheel and road are now allowed to penetrate or to separate from each other, the definition of the contact point needs to be revisited. The contact point is now defined to be the point of maximum penetration depth (even if it is negative), and it is always located on the undeformed wheel shape. It represents an approximation of the potential area of contact. This redefinition is compatible with its predecessor and therefore the equations for the contact point computation (8) are not impaired and can be maintained. One result of the computation is the determination of the penetration depth $s_n$.

The normal force $f_n$ is determined by a spring–damper system with $s_n$ as spring deformation and $\dot{s}_n$ as deformation speed. The friction characteristics remains unchanged. The elastic contact is basically specified by the spring coefficient $c_n$ and the damping coefficient $d_n$ as

$$f_n = c_n s_n + d_n \dot{s}_n. \tag{31}$$

This contact force model leads to non-physical behaviour due to the following effects:

(1) When the damper force $d_n \dot{s}_n$ becomes larger as the spring force $c_n s_n$ and with opposite sign, the contact force would be 'pulling/sticking' which is non-physical, since during contact only pushing forces can occur.
(2) When contact occurs with a non-zero relative speed (e.g. when the wheel bumps on the road), the damping force has a non-zero value and therefore the contact force changes discontinuously at $s_n = 0$. Again, this is not physical because the force can only change continuously.[1]

In the literature there are several proposals to fix the second problem. However, there seems to be no proposal to avoid sticking. For this reason, the most simple approach is used, to fix both problems by slight changes to the linear spring/damper characteristic:

$$f_n = \begin{cases} 0 & \text{if } s_n \geq 0 \text{ or } c_n s_n + d_n \dot{s}_n \leq 0, \\ c_n s_n + \min(c_n s_n, d_n \dot{s}_n) & \text{else.} \end{cases} \tag{32}$$

Note, when sticking would occur $c_n s_n + d_n \dot{s}_n \leq 0$, then the contact force is explicitly set to zero. The $\min(c_n s_n, d_n \dot{s}_n)$ part limits the damping force when it is pushing. This means that at

the start of the contact ($s_n = 0$), this term is zero and the contact force changes continuously. The effect of both modifications is that the absolute value of the damping force is always limited by the absolute value of the spring force: $|d_n \dot{s}_n| \leq |c_n s_n|$.

The force $\boldsymbol{f}_{\text{tyre}}$ acts on the projection of the virtual contact point on the road. Therefore, Equation (18) is modified to

$$\boldsymbol{t} = \boldsymbol{I}\dot{\boldsymbol{\omega}} + \boldsymbol{\omega} \times \boldsymbol{I}\boldsymbol{\omega} + \boldsymbol{R}((\boldsymbol{d}_{W,0} - s_n \cdot \boldsymbol{e}_n) \times \boldsymbol{f}_{\text{tyre},0}). \tag{33}$$

### 5.1. *Roll resistance*

Roll resistance denotes a phenomenon that represents a summarisation of numerous effects. The resistance partially results from the imperfect elastic deformation of the tyre that causes a loss of kinematic energy. Additionally, air will agglomerate at the entrance of the tread shuffle and needs to be pumped around the rim. Furthermore, the corresponding pressure peak at the shuffle entrance causes a counteracting momentum.

Disregarding this complexity, the roll resistance is mostly modelled by a single coefficient that is derived by measurement $\mu_{\text{roll}}$. This coefficient is usually given in a way that the imaginary counteracting force acting at the wheel's centre is $f_n \cdot \mu_{\text{roll}}$. In this implementation, we prefer to express the roll resistance by a counteracting torque since this includes also the component of lateral rolling. For preparation, the angular velocity $\boldsymbol{\omega}_0$ of the wheel is decomposed into a turning component $\boldsymbol{\omega}_{\text{turn}}$ and a remainder that expresses the rolling velocity $\boldsymbol{\omega}_{\text{roll}}$.

$$\boldsymbol{\omega}_{\text{turn}} = (\boldsymbol{\omega}_0 \cdot \boldsymbol{e}_n)\boldsymbol{e}_n, \tag{34}$$

$$\boldsymbol{\omega}_{\text{roll}} = \boldsymbol{\omega}_0 - \boldsymbol{\omega}_{\text{turn}}, \tag{35}$$

$$|\boldsymbol{t}_{\text{roll}}| = f_n \cdot r \cdot \mu_{\text{roll}}. \tag{36}$$

The torque counteracts $\boldsymbol{\omega}_{\text{roll}}$ and is assumed to be proportional to the normal force. Since the roll resistance introduces stiffness close to the rest state, a similar regularisation scheme as in Section 4 is applied. For small values of $\boldsymbol{\omega}_{\text{roll}}$, the counteracting torque becomes a linear function of $\boldsymbol{\omega}_{\text{roll}}$:

$$-\boldsymbol{t}_{\text{roll}} = f_n \cdot \mu_{\text{roll}} \cdot r \cdot \begin{cases} \dfrac{\boldsymbol{\omega}_{\text{roll}}}{|\boldsymbol{\omega}_{\text{roll}}|} & \text{if } r|\boldsymbol{\omega}_{\text{roll}}| > v\text{Adhesion}, \\ \dfrac{\boldsymbol{\omega}_{\text{roll}}}{v\text{Adhesion}} & \text{if } r|\boldsymbol{\omega}_{\text{roll}}| \leq v\text{Adhesion}. \end{cases} \tag{37}$$

This model of the rolling resistance is open for further extension. More accurate models [14] consider that the coefficient is rising linearly or quadratically with the wheel's rolling velocity. However, the air resistance usually becomes the major loss of energy for a vehicle at high speed and the influence of roll resistance is probable to become negligible.

The resulting model for simple slick-tyre wheels represents a freely moving body-element and owns consequently all six degrees of freedom. Hence, the wheel model has 12 potential state variables and two nonlinear algebraic equations for the contact point calculation.

## 6. Modelling of a tyre with tread (level 4)

### 6.1. *Tread handling with the approach of Rill*

The previous model applied a dry-friction model on an elastic tyre. This represents only a reasonable assumption if the tyre is slick and reasonably stiff. However, most of the tyres

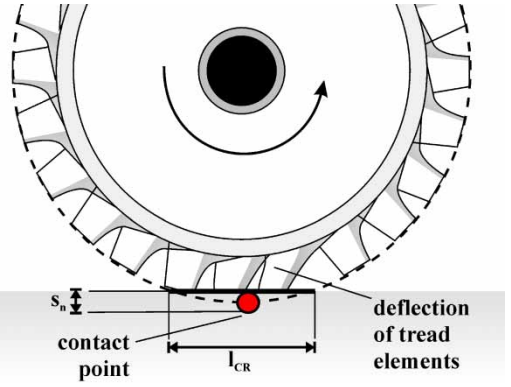


Figure 5. An illustration of the tread element's deflection within the contact area (marked by $l_{CR}$).

are elastic and the deflection of the tread elements is of major importance. Hence a closer examination at the tread shuffle is needed (Figure 5). This area surrounds the contact point and its dimensions are determined by its length $l_{\mathrm{CR}}$ in longitudinal direction and its width $w_{\mathrm{CR}}$ in lateral direction. Both variables are dependent on the wheel geometry (e.g. the radius $r$) and the penetration depth $s_{\mathrm{n}}$. Equation (38) presents a possible approximation for $l_{\mathrm{CR}}$. A similar approximation can be done for $w_{\mathrm{CR}}$.

$$l_{\mathrm{CR}} = \sqrt{8 r s_{\mathrm{n}}}, \tag{38}$$

this approximation follows out of Pythagoras' rule $(l_{CR}/2)^2 = r^2 - (r - s_{\mathrm{n}})^2$ for $s_{\mathrm{n}} \ll r$.

The bristles or tread elements that form the tread pattern undergo a deflection in the shuffle. The maximal possible deflection (maxDefl) of a tread element results from the product of the slip velocity $v\mathrm{Slip}$ and its duration of stay $t_{\mathrm{CR}}$ in the tread shuffle. This computation is based upon the presumption that the tread elements perfectly adhere to the road's surface.

$$\max \mathrm{Defl} = v\mathrm{Slip} \cdot t_{\mathrm{CR}} = v\mathrm{Slip} \frac{l_{\mathrm{CR}}}{|\boldsymbol{d}_{\mathrm{W},0} \times \boldsymbol{\omega}_0|} = v\mathrm{Slip} \frac{l_{\mathrm{CR}}}{v\mathrm{Roll}}. \tag{39}$$

The variable $v\mathrm{Roll}$ represents the roll velocity $|\boldsymbol{d}_{\mathrm{W},0} \times \boldsymbol{\omega}_0|$. To describe the friction characteristics of such a tyre, the models of Rill and Pacejka use the concept of slip (that should not be confused with the term 'slip-velocity'). The slip $S$ ($S_{\mathrm{lat}}$, $S_{\mathrm{long}}$, resp.) is defined to be the quotient of the slip velocity $v\mathrm{Slip}$ and the roll velocity $v\mathrm{Roll}$ and represents (roughly speaking) the fraction of wheel spin.

$$S = \frac{v\mathrm{Slip}}{v\mathrm{Roll}}, \tag{40}$$

$$S_{\mathrm{lat}} = v\mathrm{Slip}_{\mathrm{lat}}/v\mathrm{Roll}, \tag{41}$$

$$S_{\mathrm{long}} = v\mathrm{Slip}_{\mathrm{long}}/v\mathrm{Roll}. \tag{42}$$

The force transmission is specified for a certain load $f_{\mathrm{n}}$ by the coefficient $\mu_S$ that is dependent on the slip $S$. A typical characteristic curve for this coefficient is shown by the solid curve in Figure 6. For low slip values the presumption of perfectly adhering tread elements is valid and the transmitted force is proportional to the deflection maxDefl. Thus, the characteristic curve of $\mu_S$ is linearly rising for small slip values. The slip value $s\mathrm{Adhesion}$ specifies the point of maximal force transmission. The tread elements do not perfectly adhere to the road any more but their average deflection has reached a maximum. From there on, more and more tread elements start to slide and in consequence the coefficient's value decreases. At the slip value

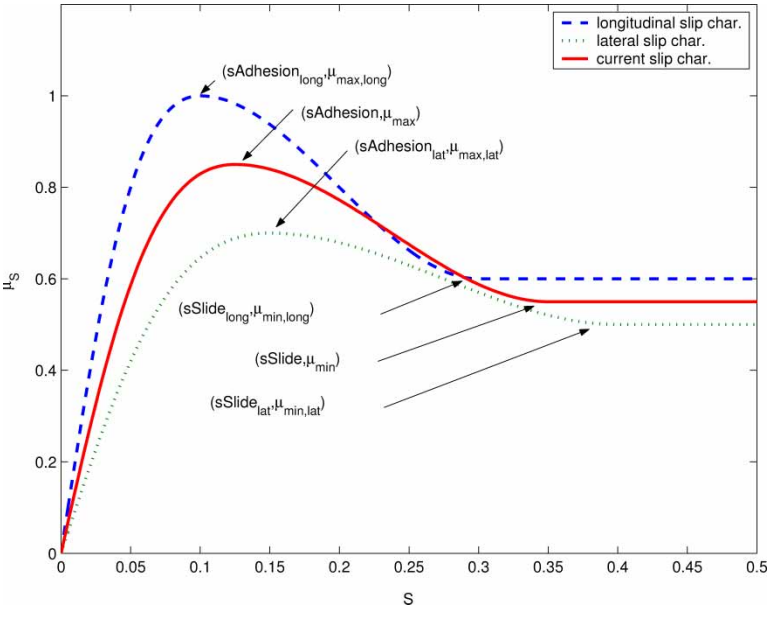


Figure 6. Characteristic curves for $\mu_S$. The dashed blue curve shows the characteristics for pure lateral slip. The behaviour for pure longitudinal slip is presented by the dotted green curve. The solid red curve presents an exemplary characteristic curve for an arbitrary slip direction.

of *s*Slide the model enters the state of full sliding friction and $\mu_S$ represents the corresponding friction coefficient that remains constant for all slip values greater than *s*Slide.

Hence the characteristic curve for $\mu_S$ can be described by two specific points: ($s$Adhesion, $\mu_{max}$) and ($s$Slide, $\mu_{min}$), using the interpolation Equation (28) of Section 4. Since the slip characteristics for longitudinal and lateral slip are mostly different, two separate characteristic curves are defined by the corresponding parameter pairs:

$$[(s\text{Adhesion}_{lat}, \mu_{max,lat}), (s\text{Slide}_{lat}, \mu_{min,lat})],$$
$$[(s\text{Adhesion}_{long}, \mu_{max,long}), (s\text{Slide}_{long}, \mu_{min,long})].$$

The behaviour for an arbitrary slip direction is then determined by the method of parameter mixing. The variable pairs ($s$Adhesion, $\mu_{max}$) and ($s$Slide, $\mu_{min}$) are dependent on the current slip direction: their corresponding lateral and longitudinal components are weighted according to the trigonometric Pythagoras:

$$s\text{Adhesion} = \sqrt{\left(\frac{v\text{Slip}_{lat}}{v\text{Slip}}\right)^2 s\text{Adhesion}_{lat}^2 + \left(\frac{v\text{Slip}_{long}}{v\text{Slip}}\right)^2 s\text{Adhesion}_{long}^2}, \tag{43}$$

$$s\text{Slide} = \sqrt{\left(\frac{v\text{Slip}_{lat}}{v\text{Slip}}\right)^2 s\text{Slide}_{lat}^2 + \left(\frac{v\text{Slip}_{long}}{v\text{Slip}}\right)^2 s\text{Slide}_{long}^2}, \tag{44}$$

$$\mu_{max} = \sqrt{\left(\frac{v\text{Slip}_{lat}}{v\text{Slip}}\right)^2 \mu_{max,lat}^2 + \left(\frac{v\text{Slip}_{long}}{v\text{Slip}}\right)^2 \mu_{max,long}^2}, \tag{45}$$

$$\mu_{min} = \sqrt{\left(\frac{v\text{Slip}_{lat}}{v\text{Slip}}\right)^2 \mu_{min,lat}^2 + \left(\frac{v\text{Slip}_{long}}{v\text{Slip}}\right)^2 \mu_{min,long}^2}. \tag{46}$$

The formulas above are from Rill [4]. They have been successfully applied in the TMeasy [3] tyre models. Hence data for the wheel specification can be shared. Although the slip is an excellent variable to find a good description of the tyre behaviour in most of the relevant cases, it unfortunately becomes an inadequate and numerical critical quantity for low rolling velocities. If the rolling velocity is close to zero even the smallest slip velocity will lead to full sliding friction. Furthermore, a division by zero occurs if the slip is zero. A possible workaround for the numerical difficulties can be obtained by adding an artificial term to the denominator of the slip definition [15]. Unfortunately, such an attempt leads inevitably to a poor accuracy for low rolling velocities.

### 6.2. *Combination of the approaches for low and high rolling velocities*

We take a new and different approach that also avoids the direct computation of the slip variables and is therefore uncritical: the dry-friction model of the previous section leads to a dependence of the friction force solely on $v$Slip. Apparently, it represents an appropriate and

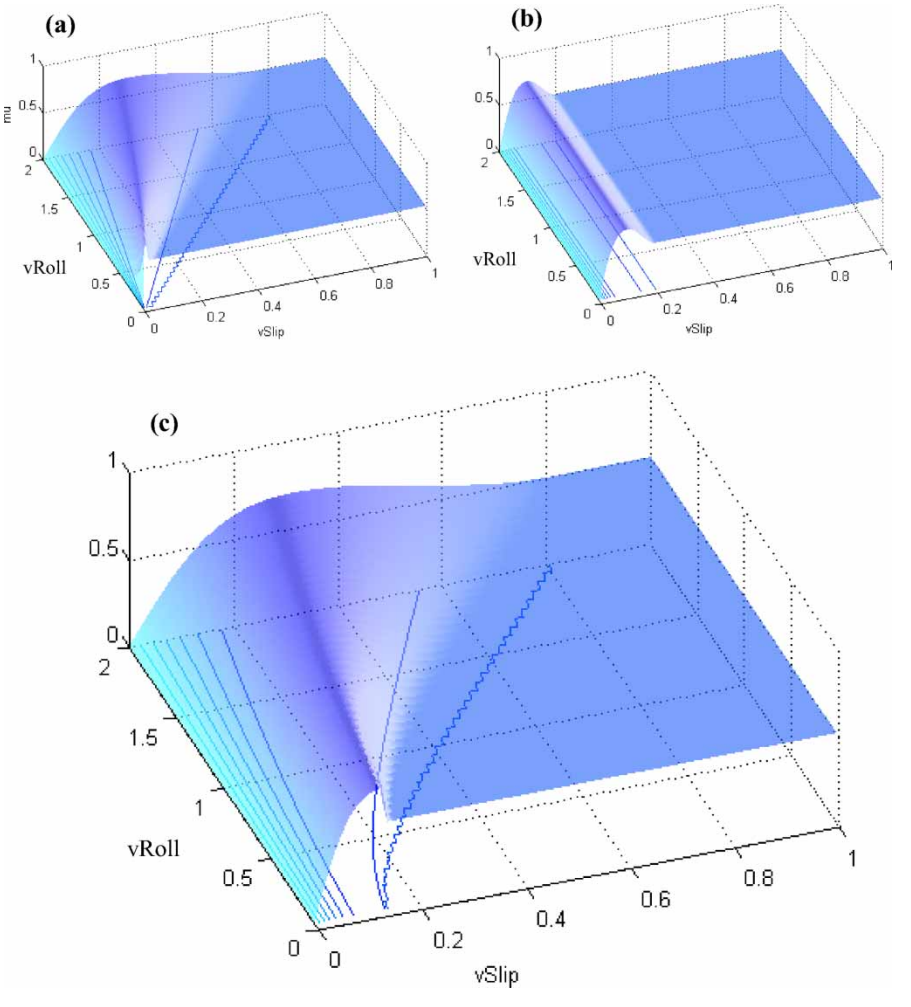


Figure 7. Different characteristic surfaces of the friction coefficient in dependence of $v$Roll and $v$Slip.

numerical stable description for low rolling velocities. Whereas the appropriate model for a low rolling velocity defines the friction coefficients on the basis of the slip velocity, the model for higher rolling velocities uses the slip as domain variable for the characteristic curve. We have now two separate models for low and high rolling velocities. Figure 7a and b shows the characteristic curves of both models in dependence of $v$Slip and $v$Roll. A parameterised transition between these models shall lead to a more general model.

A common formulation of both models can be obtained by making the points of maximal friction and sliding friction depending on the rolling velocity. Let $v$AR be the point of maximum force transmission and $v$SR the point of complete slippage. In case of a low rolling velocity, $v$AR is equal to $v$Adhesion and $v$SR is equal to $v$Slide. If the rolling velocity is high, the slip model can be activated by stating that $v$AR is equal to $s$Adhesion $\cdot\, v$Roll and $v$SRs $= s$Slide $\cdot\, v$Roll. Such a formulation of the slip model also avoids the numerical difficulties since the actual slip is not computed any more.

It is presumed that both models share the values for $\mu_{\max}$ and $\mu_{\min}$ since the actual process of rolling should not drastically influence these attributes. Hence the transition between the models can be reduced to a transition between the values for $v$AR and $v$SR. It is further presumed that an increase of rolling velocity can only raise the values of $v$AR and $v$SR. Therefore a transition by the softmax function is suggested. The softness of this transition is determined by the parameter tol.

$$v\mathrm{AR} = \mathrm{softmax}_{\mathrm{tol}}(v\mathrm{Adhesion}, s\mathrm{Adhesion} \cdot v\mathrm{Roll}), \tag{47}$$

$$v\mathrm{SR} = \mathrm{softmax}_{\mathrm{tol}}(v\mathrm{Slide}, s\mathrm{Slide} \cdot v\mathrm{Roll}), \tag{48}$$

$$\mathrm{softmax}_{\mathrm{tol}}(a, b) = \log(\mathrm{e}^{a/\mathrm{tol}} + \mathrm{e}^{b/\mathrm{tol}}) \cdot \mathrm{tol}. \tag{49}$$

The influence of $v$Slip on the friction coefficient $\mu_S$ is then modelled following the interpolation scheme of Equation (28). The resulting transition between the two models is shown in Figure 7c. Note that no longer can a division by zero occur, because for low velocities, a division by $v$Slip is no longer present (since it cancels with the same variable in the numerator of $\mu_S$).

$$\mu_S = \begin{cases} \dfrac{v\mathrm{Slip} \cdot \dot{\mu}_{v\mathrm{Slip}}(0)}{1 + \sigma((v\mathrm{AR}/\mu_{\max})\dot{\mu}_{v\mathrm{Slip}}(0) - 2 + \sigma)}, & v\mathrm{Slip} \le v\mathrm{AR}, \\ & \sigma = \dfrac{v\mathrm{Slip}}{v\mathrm{AR}}, \\ \mu_{\max} - (\mu_{\max} - \mu_{\min})\sigma^2(3 - 2\sigma), & v\mathrm{AR} < v\mathrm{Slip} < v\mathrm{SR}, \\ & \sigma = \dfrac{v\mathrm{Slip} - v\mathrm{AR}}{v\mathrm{SR} - v\mathrm{AR}}, \\ \mu_{\min}, & v\mathrm{SR} \le v\mathrm{Slip}, \end{cases} \tag{50}$$

$$f_{\mathrm{lat}} = f_{\mathrm{n}} \left( \frac{\mu_S}{v\mathrm{Slip}} \right) v\mathrm{Slip}_{\mathrm{lat}}, \tag{51}$$

$$f_{\mathrm{long}} = f_{\mathrm{n}} \left( \frac{\mu_S}{v\mathrm{Slip}} \right) v\mathrm{Slip}_{\mathrm{long}}. \tag{52}$$

### 6.3. *Nonlinear influence of the normal load*

All friction forces ($f_{\mathrm{lat}}$ and $f_{\mathrm{long}}$) are defined to be linearly dependent on the normal load $f_{\mathrm{n}}$ so far. Since a tyre is a deformable object, its friction characteristic changes in dependence

on the deformation due to a higher normal load and the pressure distribution within the tread shuffle becomes increasingly less uniform. At the entrance and at the exit of the tread shuffle, the pressure is too low to significantly deflect the tread elements. A potential pressure peak in the front part of the shuffle cannot effectively transmit the force because of the low deflection at this position. Therefore the forces are increasing less than linear with respect to the normal load and the corresponding friction coefficients are decreasing. To model this nonlinearity the friction coefficients are changed to be a function of $f_n$.

The model of the nonlinear influence of the normal load is according to a proposal by Rill [4]. According to our framework, it is here applied on the coefficients and not directly on the transmission forces. It is based upon two points of measurement $\mu_1$ and $\mu_2$ for an arbitrary friction coefficient $\mu$: $\mu_1$ is given for $f_n = f_{n,1}$ and $\mu_2$ is given for $f_n = f_{n,2} = 2f_{n,1}$. The dependence of $\mu$ on $f_n$ is then modelled by the algebraic most simple construct: a linear interpolation:

$$\mu = (2\mu_1 - \mu_2) - (\mu_1 - \mu_2)\frac{f_n}{f_{n,1}}. \tag{53}$$

The resulting friction force $f_n \cdot \mu$ is then a quadratic function of $f_n$ with a peak at $f_{n,sat}$. For all $f_n > f_{n,sat}$ the friction force equals the maximum force at the peak and the coefficient $\mu$ is determined in this case by Equation (54) and no longer by Equation (53).

$$\mu = \frac{(2\mu_1 - \mu_2)^2}{4(\mu_1 - \mu_2)}\frac{f_{n,1}}{f_n} \quad \text{if } f_n > f_{n,sat} = \frac{f_{n,1}(2\mu_1 - \mu_2)}{2(\mu_1 - \mu_2)}. \tag{54}$$

This dependency concerns the friction coefficients $\mu_{max,lat}$, $\mu_{max,long}$, $\mu_{min,lat}$, $\mu_{min,long}$ and $\mu_{turn}$ (that will appear later) to be dependent on $f_n$ as defined in Equations (53) and (54). In addition, the parameters $s\text{Slide}_{lat}$, $s\text{Adhesion}_{lat}$, $s\text{Slide}_{long}$ and $s\text{Adhesion}_{long}$ are assumed to be linearly depending on the normal load. Having given also these values at $f_n = f_{n,1}$ and $f_n = f_{n,2}$ the dependency can simply be modelled by a linear approximation.

### 6.4. *Lateral slip due to camber inclination*

A tilt of the wheel with respect to the road plane causes an additional lateral deflection of the tread elements. This process is illustrated in Figure 8. Due to the (potential) adhesion of the tread elements within the contact patch, the tread elements are bounded to stay near their entrance point and cannot move on their natural path. Since the slip is proportional to potential deflection, the influence of camber can be modelled by the addition of a lateral camber slip. This principal idea has been outlined by Pacejka [1] and Rill [4]. The corresponding sets of

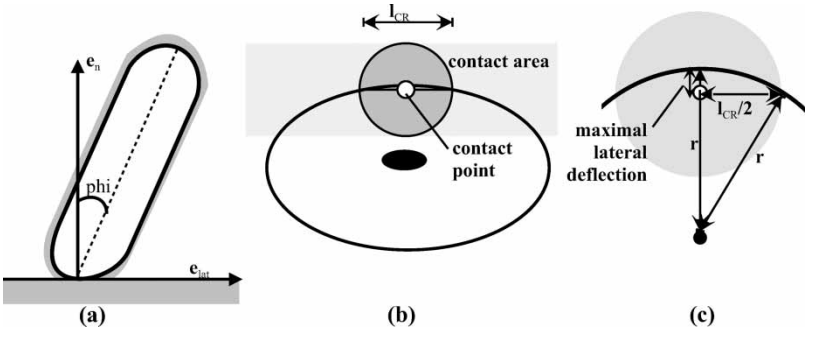


Figure 8. Different views of a tilted wheel: (a) side view, (b) top view and (c) the maximum deflection.

equations depend then on their given models. Also here, we derive a new set of equations that better suits our framework.

The maximum camber deflection is depicted in Figure 8c. The corresponding formula (56) is derived by trigonometric rules. The effective deflection is then derived through the tilt angle $\varphi$. The influence of camber is therefore dependent on the tilt angle and on the length of the contact region that is determined by geometry and penetration depth.

$$\text{maxCamberDefl} = r - r\sqrt{1 - \left(\frac{l_{\text{CR}}}{2r}\right)^2}, \tag{55}$$

$$\text{camberDefl} = \sin(\varphi) \cdot \text{maxCamberDefl}. \tag{56}$$

This lateral deflection is transformed into an additional lateral slip by a scaling factor $\text{gain}_{\text{camber}}$ that has to be specified. The product of this slip and the rolling velocity $v\text{Roll}$ forms the corresponding slip velocity camberVSlip. Hence, Equation (19) that concerns the lateral slip velocity is modified accordingly. This approach uses a combined slip model that integrates well into the existing set of equations, takes various influences into account and is robust.

$$\text{camberVSlip} = v\text{Roll} \cdot \text{gain}_{\text{camber}} \cdot \text{camberDefl}, \tag{57}$$

$$v\text{Slip}_{\text{lat}} = (\boldsymbol{v}_0 + \boldsymbol{\omega}_0 \times \boldsymbol{d}_{\text{W},0}) \cdot \boldsymbol{e}_{\text{lat}} + \text{camberVSlip}. \tag{58}$$

### 6.5. *Self-aligning torque*

The distribution of lateral shear stress within the tread shuffle changes in dependence of the driving situation. According to Rill [4] there is usually a pressure peak in longitudinal direction behind the contact point in the case of normal adhesive rolling. In the transition between rolling and sliding it moves in front of the contact point and becomes equal to contact point in the case of complete slippage. This positional shift of the pressure peak is denoted with $l_{\text{trail}}$ and can be approximated by the following empirical formula:

$$l_{\text{trail}} = \begin{cases} \dfrac{1}{6} l_{\text{CR}} \left(1 - \dfrac{v\text{Slip}_{\text{lat}}}{v\text{AR}}\right) & \text{if } v\text{Slip}_{\text{lat}} \leq v\text{AR}, \\ \dfrac{-1}{6} l_{\text{CR}} \dfrac{v\text{Slip}_{\text{lat}} - v\text{AR}}{v\text{AR}(v\text{SR} - v\text{Slip}_{\text{lat}}/v\text{SR} - v\text{AR})^2} & \text{if } v\text{AR} < v\text{Slip}_{\text{lat}} < v\text{SR}, \\ 0 & \text{else.} \end{cases} \tag{59}$$

The positional shift $l_{\text{trail}}$ determines the point of application for the lateral force $f_{\text{lat}}$. This causes a self-aligning torque $\boldsymbol{t}_{\text{SA}}$ in the direction of $\boldsymbol{e}_{\text{n}}$. The parameter $\text{gain}_{\text{SA}}$ is a scaling factor to model the strength of this effect.

$$\boldsymbol{t}_{\text{SA}} = \text{gain}_{\text{SA}}(-\text{sign}_{\text{trail}} l_{\text{trail}} \boldsymbol{e}_{\text{long}} \times f_{\text{lat}} \boldsymbol{e}_{\text{lat}}). \tag{60}$$

The product of signTrail and $\boldsymbol{e}_{\text{long}}$ determines the normalised projection of the rolling velocity on the longitudinal direction. Since the resulting torque $\boldsymbol{t}_{\text{SA}}$ becomes a stiff variable for small rolling velocities, the standard regularisation is applied if the projection of the rolling velocity on $\boldsymbol{e}_{\text{long}}$ is smaller than $v\text{Adhesion}$.

$$\text{sign}_{\text{trail}} = \begin{cases} \text{sign}((\boldsymbol{\omega}_0 \times \boldsymbol{W}_0) \cdot \boldsymbol{e}_{\text{long}}) & \text{if } (\boldsymbol{\omega}_0 \times \boldsymbol{W}_0) \cdot \boldsymbol{e}_{\text{long}} > v\text{Adhesion}, \\ (\boldsymbol{\omega}_0 \times \boldsymbol{W}_0) \cdot \dfrac{\boldsymbol{e}_{\text{long}}}{v\text{Adhesion}} & \text{else.} \end{cases} \tag{61}$$

### 6.6. *Bore torque*

In Section 5.1, the angular velocity has been decomposed into $\boldsymbol{\omega}_{\text{roll}}$ and $\boldsymbol{\omega}_{\text{turn}}$. Whereas the rolling component is counteracted by the friction torque of roll resistance, there is also a counteracting torque for the turning component. The turning resistance is mainly dependent on the geometry of the contact patch, and on the current driving situation. A slim, fast rolling bicycle wheel is easier to turn (to steer, resp.) than a wider truck wheel at rest. The turning leads to an additional deflection of the tread elements within the contact patch. The strength of this deflection is proportional to the distance $s$ of the tread element to the virtual contact point (cf. Figure 9). To this end, previous computational schemes of Rill [4] have been adapted to our framework.

The slip velocity of a tread element with distance $s = \sqrt{x^2 + y^2}$ is $|\boldsymbol{\omega}_{\text{turn}}| \cdot s$. The corresponding force is expected to have a similar characteristic as the transmission forces for the longitudinal and lateral slip velocity. But for the sake of simplicity, the friction force is described as a limited linear function. The force is linearly increasing until it reaches a level of saturation at $\min(f_{\text{n}}\mu_{\text{turn}}|\boldsymbol{\omega}_{\text{turn}}|s/v\text{AR}, f_{\text{n}}\mu_{\text{turn}})$, where $\mu_{\text{turn}}$ represents the corresponding friction coefficient.

The overall resistance torque $|t_{\text{turn}}|$ is determined by summation of the forces on all the tread elements. It is presumed that $|\boldsymbol{\omega}_{\text{turn}}| \cdot s$ is always smaller than $v\text{AR}$:

$$
\begin{aligned}
|\boldsymbol{t}_{\text{turn}}| &= \int_{-l_{\text{CR}}/2}^{l_{\text{CR}}/2} \int_{-w_{\text{CR}}/2}^{w_{\text{CR}}/2} s \frac{f_{\text{n}}}{l_{\text{CR}} w_{\text{CR}}} \mu_{\text{turn}} \frac{|\boldsymbol{\omega}_{\text{turn}}|}{v\text{AR}} s \,\text{d}y\,\text{d}x \\
&= \frac{4}{l_{\text{CR}} w_{\text{CR}}} f_{\text{n}} \mu_{\text{turn}} \frac{|\boldsymbol{\omega}_{\text{turn}}|}{v\text{AR}} \int_0^{l_{\text{CR}}/2} \int_0^{w_{\text{CR}}/2} s^2 \,\text{d}y\,\text{d}x \\
&= \frac{1}{12} (l_{\text{CR}}^2 + w_{\text{CR}}^2) f_{\text{n}} \mu_{\text{turn}} \frac{|\boldsymbol{\omega}_{\text{turn}}|}{v\text{AR}}, \qquad (62)
\end{aligned}
$$

$$
|\boldsymbol{t}_{\text{turn}}| = \sqrt{\frac{l_{\text{CR}}}{12^2} + \frac{w_{\text{CR}}}{12^2}} f_{\text{n}} \mu_{\text{turn}} \frac{|\boldsymbol{\omega}_{\text{turn}}| \sqrt{l_{\text{CR}}/12^2 + w_{\text{CR}}/12^2}}{v\text{AR}}, \qquad (63)
$$

$$
|\boldsymbol{t}_{\text{turn}}| \approx \frac{1}{4} \sqrt{l_{\text{CR}}^2 + w_{\text{CR}}^2} f_{\text{n}} \mu_{\text{turn}} \frac{|\boldsymbol{\omega}_{\text{turn}}| (1/4) \sqrt{l_{\text{CR}}^2 + w_{\text{CR}}^2}}{v\text{AR}}. \qquad (64)
$$

The transformation from Equation (62) to Equation (63) just represents a rearrangement of the final result. The latter equation is of the same form as the computation for the turning resistance for a single tread element. Hence the friction torque $\boldsymbol{t}_{\text{turn}}$ can be interpreted as the

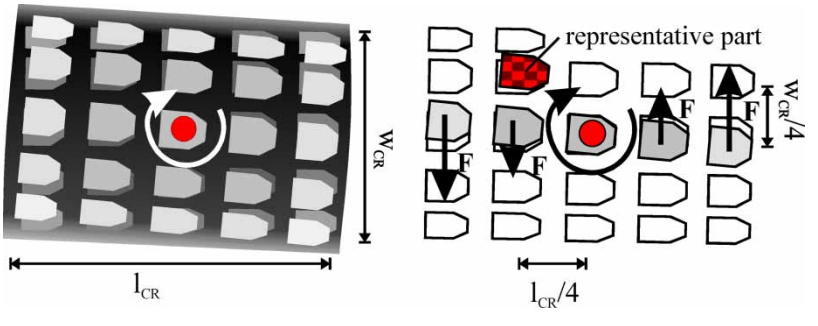


Figure 9. The two views of the contact region show the deflection of the tread elements due to the turning of the wheel. In (b) the representative part is marked and the forces on the single tread elements are depicted.

torque on a single representative part with distance $s \approx 1/4\sqrt{l_{\mathrm{CR}}^2 + w_{\mathrm{CR}}^2}$ to the contact point. Equation (63) holds if the velocity of the representative part allows the tread element to adhere. When the slip velocity of the representative part exceeds the corresponding threshold value $v\mathrm{AR}$, the tread elements start to slide and the turning friction remains by definition on its level of saturation.

$$-\boldsymbol{t}_{\mathrm{turn}} = \begin{cases} \hat{f}_{\mathrm{n}}\mu_{\mathrm{turn}}\dfrac{1}{16}\left(l_{\mathrm{CR}}^2 + w_{\mathrm{CR}}^2\right)\dfrac{\boldsymbol{\omega}_{\mathrm{turn}}}{v\mathrm{AR}} & \text{if } |\boldsymbol{\omega}_{\mathrm{turn}}|\dfrac{1}{4}\sqrt{l_{\mathrm{CR}}^2 + w_{\mathrm{CR}}^2} \le v\mathrm{AR}, \\ \hat{f}_{\mathrm{n}}\mu_{\mathrm{turn}}\dfrac{1}{4}\sqrt{l_{\mathrm{CR}}^2 + w_{\mathrm{CR}}^2}\dfrac{\boldsymbol{\omega}_{\mathrm{turn}}}{|\boldsymbol{\omega}_{\mathrm{turn}}|} & \text{else.} \end{cases} \tag{65}$$

All these different aspects of tyre behaviour that have been added to the model of level 3 lead to a number of straightforward calculations. The model does not introduce new differential equations or new implicit algebraic equations. Hence, the model complexity with respect to the set of state variables remains unaffected.

## 7. Implicit modelling of the tyre deformation (levels 5 and 6)

The lateral and longitudinal deformation of the tyre can be modelled with a virtual spring–damper system, as presented in Figure 10. The spring deflection is denoted by $s_{\mathrm{lat}}$ and $s_{\mathrm{long}}$, respectively. The corresponding spring–damper equations relate these two variables to the tyre forces. The parameters $c_{\mathrm{lat}}$, $c_{\mathrm{long}}$ and $d_{\mathrm{lat}}$, $d_{\mathrm{long}}$ denote the spring and damper coefficients.

$$f_{\mathrm{lat}} = c_{\mathrm{lat}}s_{\mathrm{lat}} + d_{\mathrm{lat}}\dot{s}_{\mathrm{lat}}, \tag{66}$$

$$f_{\mathrm{long}} = c_{\mathrm{long}}s_{\mathrm{long}} + d_{\mathrm{long}}\dot{s}_{\mathrm{long}}. \tag{67}$$

The lateral and longitudinal deformation influences the slip velocity and therefore Equations (58) and (19) have to be modified:

$$(\boldsymbol{v}_0 + \boldsymbol{\omega}_0 \times \boldsymbol{d}_{\mathrm{W},0}) \cdot \boldsymbol{e}_{\mathrm{lat}} + \mathrm{camber}V\mathrm{Slip} = v\mathrm{Slip}_{\mathrm{lat}} - \dot{s}_{\mathrm{lat}}, \tag{68}$$

$$(\boldsymbol{v}_0 + \boldsymbol{\omega}_0 \times \boldsymbol{d}_{\mathrm{W},0}) \cdot \boldsymbol{e}_{\mathrm{long}} = v\mathrm{Slip}_{\mathrm{long}} - \dot{s}_{\mathrm{long}}. \tag{69}$$

The nonlinear dependency between $v\mathrm{Slip}_{\mathrm{lat}}$ and $f_{\mathrm{lat}}$ can no longer be explicitly solved for $f_{\mathrm{lat}}$. Instead, both $vSlip_{\mathrm{lat}}$ and $f_{\mathrm{lat}}$ are now part of an algebraic loop and must be solved during

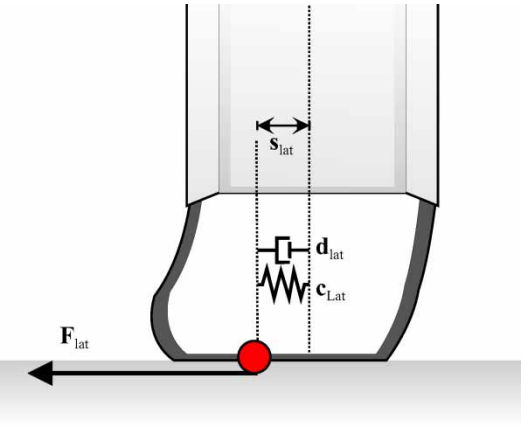


Figure 10. The lateral deformation of a tyre is modelled by a virtual spring–damper system.

the simulation together with Equations (66) and (68). The same holds for the corresponding equations in longitudinal direction. Hence two new, nonlinear algebraic equations have to be solved during simulation. The state variables remain unaffected and are the same as in levels 3 and 4.

### 7.1. *Linearised solution (level 5)*

The occurrence of nonlinear algebraic equations can be avoided by the application of a linearisation scheme that was presented by Rill [4] and is adapted here to our model. Since the static solution ($\dot{s}_{\text{lat}} = 0$) is easy to determine, the force $f_{\text{lat}}$ is approximated by the first two terms of the corresponding Taylor series:

$$f_{\text{lat}} \approx f_{\text{lat}}|_{\dot{s}_{\text{lat}}=0} + \left.\frac{df_{\text{lat}}}{d\dot{s}_{\text{lat}}}\right|_{\dot{s}_{\text{lat}}=0} \cdot \dot{s}_{\text{lat}} \tag{70}$$

The derivative $(\mathrm{d}f_{\text{lat}}/\mathrm{d}\dot{s}_{\text{lat}})|_{\dot{s}_{\text{lat}}=0}$ can be derived from:

$$\begin{aligned}
\frac{\mathrm{d}f_{\text{lat}}}{\mathrm{d}\dot{s}_{\text{lat}}} &= \frac{\mathrm{d}(f_{\text{n}}\mu_{v\text{Slip}}(v\text{Slip}_{\text{lat}}/v\text{Slip}))}{\mathrm{d}\dot{s}_{\text{lat}}} \\
&= f_{\text{n}}\frac{v\text{Slip}_{\text{lat}}}{v\text{Slip}}\frac{\mathrm{d}\mu_{v\text{Slip}}}{\mathrm{d}\dot{s}_{\text{lat}}} + \underbrace{f_{\text{n}}\mu_{v\text{Slip}}}_{\sqrt{f_{\text{lat}}^2+f_{\text{long}}^2}}\frac{\mathrm{d}(v\text{Slip}_{\text{lat}}/v\text{Slip})}{\mathrm{d}\dot{s}_{\text{lat}}} \\
&= -f_{\text{n}}\frac{v\text{Slip}_{\text{lat}}}{v\text{Slip}}\frac{\mathrm{d}\mu_{v\text{Slip}}}{\mathrm{d}v\text{Slip}}\underbrace{\frac{\mathrm{d}v\text{Slip}}{\mathrm{d}\dot{s}_{\text{lat}}}}_{\frac{v\text{Slip}_{\text{lat}}}{v\text{Slip}}} + \sqrt{f_{\text{lat}}^2+f_{\text{long}}^2}\frac{\mathrm{d}(v\text{Slip}_{\text{lat}}/v\text{Slip})}{\mathrm{d}\dot{s}_{\text{lat}}} \\
&= -f_{\text{n}}\left(\frac{v\text{Slip}_{\text{lat}}}{v\text{Slip}}\right)^2\frac{\mathrm{d}\mu_{v\text{Slip}}}{\mathrm{d}v\text{Slip}} - \sqrt{f_{\text{lat}}^2+f_{\text{long}}^2}\frac{v\text{Slip} - (v\text{Slip}_{\text{lat}}^2/v\text{Slip})}{v\text{Slip}^2} \\
&= -f_{\text{n}}\left(\frac{v\text{Slip}_{\text{lat}}}{v\text{Slip}}\right)^2\frac{\mathrm{d}\mu_{v\text{Slip}}}{\mathrm{d}v\text{Slip}} - \sqrt{f_{\text{lat}}^2+f_{\text{long}}^2}\frac{(v\text{Slip}_{\text{long}}/v\text{Slip})^2}{v\text{Slip}}.
\end{aligned} \tag{71}$$

The term $\mathrm{d}\mu_{v\text{Slip}}/\mathrm{d}v\text{Slip}$ can be determined by taking the derivative of the piecewise polynomial interpolation formula (50). Equation (70) represents a substitution for $f_{\text{lat}}$ that can be applied to Equation (66) to form Equation (72). This equation is then used to determine $\dot{s}_{\text{lat}}$,

$$f_{\text{lat}}|_{\dot{s}_{\text{lat}}=0} = c_{\text{lat}}s_{\text{lat}} + \underbrace{\left(\mathrm{d}_{\text{lat}} - \left.\frac{\mathrm{d}f_{\text{lat}}}{d\dot{s}_{\text{lat}}}\right|_{\dot{s}_{\text{lat}}=0}\right)}_{D}\cdot\dot{s}_{\text{lat}}. \tag{72}$$

The term $D = \mathrm{d}_{\text{lat}} - (\mathrm{d}f_{\text{lat}}/\mathrm{d}\dot{s}_{\text{lat}})|_{\dot{s}_{\text{lat}}=0}$ should not become negative to avoid heavy oscillations due to the linearisation. Therefore the term $(\mathrm{d}\mu_{v\text{Slip}}/\mathrm{d}v\text{Slip})$ is artificially limited to positive values. This leads to an inaccurate behaviour in the transition phase between adhesion and sliding, but the behaviour will always be good natured. Since the terms $f_{\text{lat}}|_{\dot{s}_{\text{lat}}=0}$, $(\mathrm{d}f_{\text{lat}}/\mathrm{d}\dot{s}_{\text{lat}})|_{\dot{s}_{\text{lat}}=0}$ and $\dot{s}_{\text{lat}}$ do all now represent known terms, Equation (70) can be used to determine $f_{\text{lat}}$. The same linearisation scheme is also applied on the variables and equations of the longitudinal direction. The resulting model can be computed in a straightforward way and no longer has nonlinear algebraic equations (with the exception of the algebraic equations to compute the contact point; as sketched in Section 2, this non-algebraic equation system can be solved in an approximative way by the non-iterative equations (12)–(14))

## 8. Explicit modelling of the tyre deformation (level 7)

The previous section modelled only the influence of the deformation on the slip velocity; the actual shift of the contact point was not taken into account. Thus, we say that the deformation of the tyre was only modelled implicitly. An explicit model also describes the contact point shift due to the tyre deformation. This can be achieved by decomposing the wheel into two idealised parts: the rim and the tyre.

The rim has the total mass and inertia of the wheel, whereas the tyre is modelled as a massless object that determines the forces acting on it according to its position and velocity. The rim and the tyre are connected with two prismatic spring–damper joints in longitudinal and lateral direction (again specified by $c_{\text{long}}$, $d_{\text{long}}$, $c_{\text{lat}}$, $d_{\text{lat}}$). This spring–damper system is modelled by equations similar to Equations (66) and (67). To achieve this decomposition, it is sufficient to introduce two new variables which replace $\boldsymbol{C}_0$ and $\boldsymbol{v}_0$ for the tyre component: $\boldsymbol{C}_0^*$ and $\boldsymbol{v}_0^*$ .

$$\boldsymbol{C}_0^* = \boldsymbol{C}_0 + s_{\text{lat}}\boldsymbol{e}_{\text{lat}} + s_{\text{long}}\boldsymbol{e}_{\text{long}}, \tag{73}$$

$$\boldsymbol{v}_0^* = \dot{\boldsymbol{C}}_0^*. \tag{74}$$

All the occurrences of $\boldsymbol{C}_0$ and $\boldsymbol{v}_0$ in the equations for contact point and slip velocity determination have to be replaced by $\boldsymbol{C}_0^*$ and $\boldsymbol{v}_0^*$ . To model the spring–damper system we use again Equations (66) and (67). From the equations for the body dynamics only the equation concerning the torque (18) and (33) is modified:

$$\boldsymbol{t} = \boldsymbol{I}\cdot\dot{\boldsymbol{\omega}} + (\boldsymbol{\omega}\times\boldsymbol{I}\cdot\boldsymbol{\omega}) + \boldsymbol{R}((\boldsymbol{C}_0^* - \boldsymbol{C}_0 + \boldsymbol{d}_{\text{W},0} - s_{\text{n}}\cdot\boldsymbol{e}_{\text{n}})\times\boldsymbol{f}_{\text{tyre},0}). \tag{75}$$

In contrast to the models of levels 5 and 6, the length variables of the virtual tyre springs are new state variables. The model therefore contains in total 14 state variables, two nonlinear algebraic equations to compute $f_{\text{lat}}$, $f_{\text{long}}$ and two nonlinear algebraic equations to determine the contact point.

## 9. Implementation in Modelica

The preceding step by step development of models for wheels and tyres has finally led to seven models with an increasing level of complexity, as summarised in Table 2. Column ‘states’ provides the number of states, or equivalently, the number of differential equations for the particular model level. Column ‘algebraic equations’ provides the number of nonlinear, algebraic equations for the particular model level. Note that two nonlinear equations are always present for the contact point calculation. These nonlinear equations reduce to a linear system in case of a planar road.

An implementation of these models is provided in the object-oriented modelling language Modelica [10]. It represents an open standard for equation-based modelling that is supported by various free and commercial M&S-environments. One of them is Dymola [16], the environment we use. The wheel models use the connectors of the free Modelica MultiBody library [11] and can therefore be conveniently integrated in a three-dimensional mechanical model. Figure 11 presents the exemplary model diagram of an uncontrolled bicycle. It is mainly built up with MultiBody components. The bicycle frame including the revolute joints consists of MultiBody elements and is directly connected to the two wheel models. More complex models (e.g. a vehicle model) can be created in a similar manner [1].

Table 2. The different wheel model levels.

| Level | Description | No. of states | No. of algebraic equations |
|---|---|---|---|
| 1 | Ideal rolling wheel | 8 | 3 |
| 2 | Rigid wheel with slip | 10 | 3 |
| 3 | Simple slick-tyre wheel | 12 | 2 |
| 4 | Simple tread-tyre wheel | 12 | 2 |
| 5 | Tread-tyre wheel with implicit deformation (linearised solution) | 12 | 2 |
| 6 | Tread-tyre wheel with implicit deformation | 12 | 4 |
| 7 | Tread-tyre wheel with explicit (contact point shift) deformation | 14 | 4 |

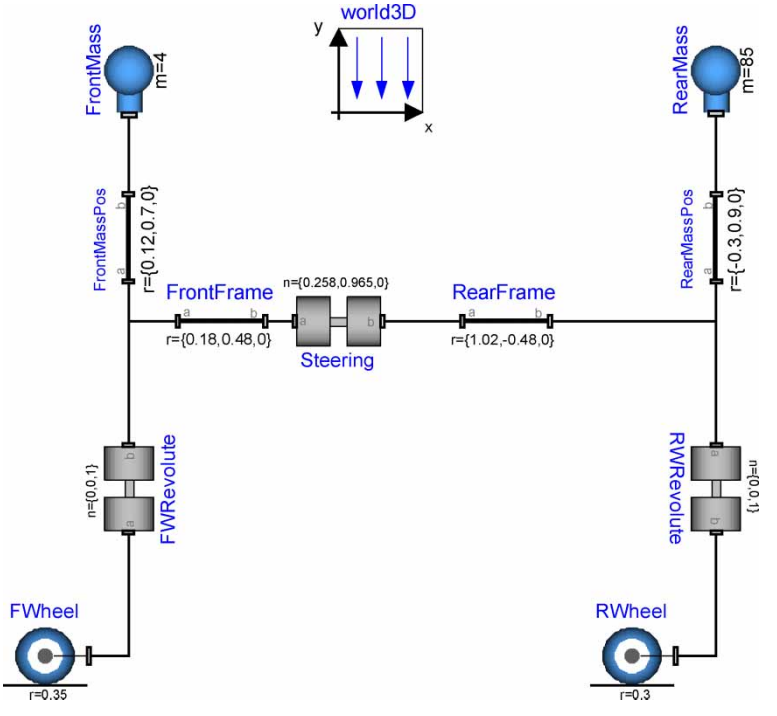


Figure 11. Modelica diagram of an uncontrolled bicycle as it appears in the schematic editor of Dymola.

The organisation of the different wheel models within an object-orientated modelling framework is an important subject. Modelica offers object-oriented means for the inclusion of sub-models, the extension of base models by inheritance, as well as replacement of used sub-models. The object-oriented structure of the wheel models is depicted in the diagram of Figure 12. Each of the presented wheel models forms a separate model. A partial sub-model *WheelBase* reduces drastically the redundancy between these models. This partial model is the base class of all the wheel models and contains their common parts. It implements the fundamental equation of motion for one wheel and the corresponding mechanism that allows an appropriate selection of the state variables. The computation of the contact point is also implemented in this partial model. Three different kinds of wheel shapes are supported and feature a suitable visualisation. This includes also a visualisation for the contact point and the corresponding contact forces.

Model *MultiLevelWheel* is the final model and represents a supermodel. It provides a general user interface for all wheel models and enables a convenient selection of the model

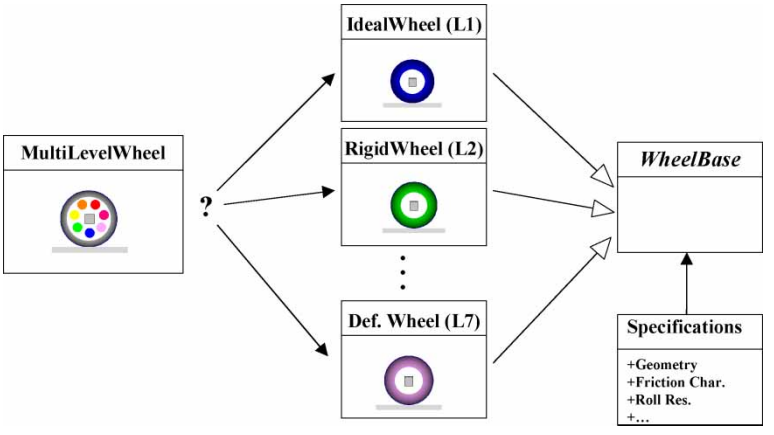


Figure 12. Diagram of the object-oriented model structure.

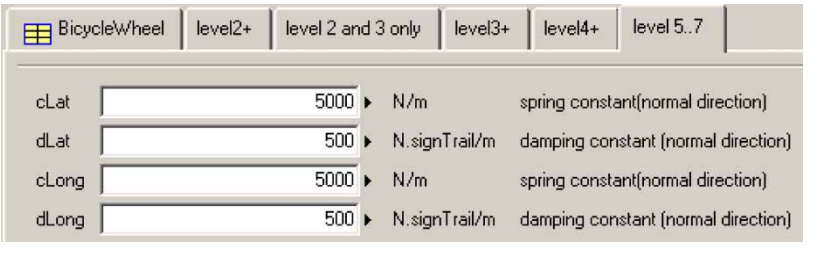


Figure 13. Parameter menu of a multi-level wheel model.

level. This supermodel can be regarded as a selective wrapper: it contains all single level models in a conditional form, so that only one of the wheel models will finally be activated. The user can select the activated sub-model by means of a parameter menu. The wheel geometry and tyre specifications are organised in separate data records. This offers a convenient way to use the same data for several model instances. The record contains all relevant parameters for all levels of complexity. Which of these parameters are finally relevant for the specific model is automatically derived in dependence of the selected level of complexity. A typical screenshot of the graphical user interface for the multi-level wheel data is shown in Figure 13. Data for the different model levels can be defined by selecting the appropriate 'tab'. For example, under tab 'level 4+' additional data can be defined for level 4 and all higher levels.

## 10. Application examples

This section demonstrates the application of the *MultiLevelWheel* model and how it can be conveniently used to examine the influence of different tyre-models on the behaviour of the overall system. Therefore, we present two rather simple experiments that consist of bicycle models that are examined in different driving scenarios. The simulations are based on models similar to Figure 11 and have been performed in Dymola using the standard solvers and integrators. All the simulations have been significantly faster than real time on a common PC. The data for the bicycle's specification has been taken from Schwab [17].

The target in both experiments is to determine the appropriate level of complexity for the tyre models. The *MultiLevelWheel* model provides a convenient tool for model selection and can thereby help the modeller to accomplish this task.

Let us start with the first experiment. We examine the braking process of a bicycle. The bicycle has an initial velocity of 10 m/s. First, the brakes are applied on the front wheel. This causes a significant balance change. In the second stage of the experiment, the rear brakes are activated. This leads to a locked rear wheel. Finally, the front brakes are released and the resulting balance shift causes the rear wheel to unlock.

The bicycle has been simulated with all presented levels of complexity and Figure 14 presents the corresponding results. Obviously, level 1 that represents an ideal rolling wheel is completely inappropriate for this manoeuvre since it is impossible to have a blocking wheel. A simulation with a level 2 model yields usable results, but due to the negligence of the tyre-deformation the balance shift is modelled inaccurately. From level 3 upwards, there is hardly any noticeable difference on the bicycle's braking characteristics. The introduction of normal deformation is sufficient to model the balance shift correctly. It turns out that already a fairly simple model is fully sufficient for this test case. Higher levels (4 and upwards) represent overkill for this experiment.

In the second experiment, we examine the self-stabilising behaviour of an uncontrolled bicycle. This behaviour emerges for a certain range of driving velocities [18]. In this stable region, the bicycle will self-stabilise into an upright driving position of lean-angle zero. The stable region is determined essentially by the mass distribution and geometry of the bicycle. Nevertheless, the tyre characteristics will also play an important role. Figure 15 depicts the stable regions for levels 1, 3, 4 and 6.

Obviously, the contact model influences drastically the system's behaviour. Each level of complexity adds additional softness to the model in terms of friction and elasticity. This influences the stability of the bicycle. The increase in elasticity delays the counteracting forces and shifts the lower bound of stability upwards. Friction and slippage have a damping effect that makes the vehicle much more stable at high speed. The conclusion is that complex tyre models are needed for the simulation of manoeuvres with high velocities. Nonetheless, it can

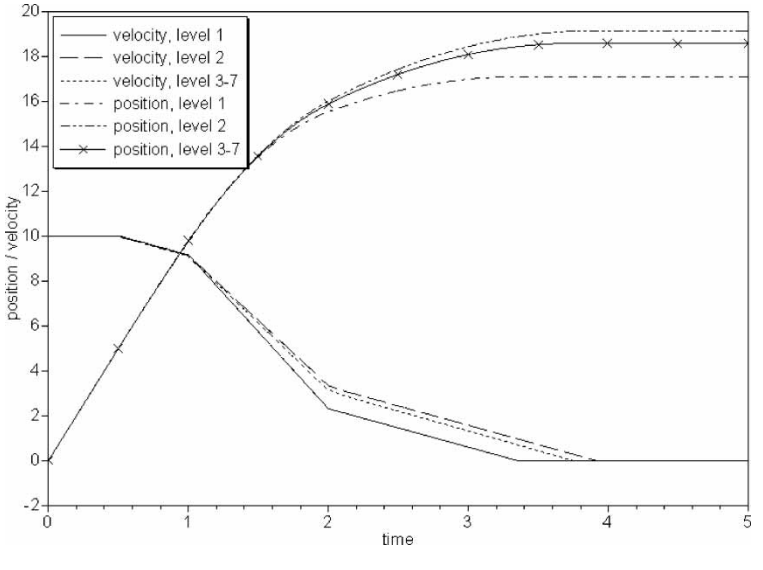


Figure 14. Braking process of the bicycle for different wheel models.

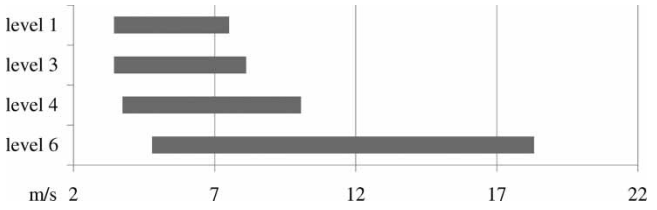


Figure 15. Stable range of the bicycle.

still be meaningful to perform experiments with idealised wheels as done in [17,18] to examine and describe the principal behaviour.

## 11. Conclusions

An object-oriented approach to tyre-modelling based on existing semi-empirical models has been presented. The stepwise refinement of the different models provides benefit for didactic purposes and eases further development. The uniform interface enables a highly convenient model selection that helps the modeller to find the appropriate level of complexity. The implementation in Modelica takes advantage of modern simulation technology and enables an integration into the existing modelling environments for multi-body and vehicle systems. The implementation goes along with a proper documentation, parameter menus and a visualisation for 3D-animations. The implementation is open for future elaboration and validation. Higher degrees of specialisation can be aspired to and integrated into the existing framework.

## Acknowledgements

We would like to express our gratitude towards Professor Karl J. Åström for the initiation of this project. Also, we would like to thank Professor François E. Cellier for his continuing interest and support.

## Note

1. This contact model is not an idealised model where a steep characteristic is approximated by a discontinuity, but it shall model the steep characteristic.

## References

[1] H.B. Pacejka, *Tire and Vehicle Dynamics*, Elsevier BH, Amsterdam, 2006.
[2] W. Hirschberg, G. Rill, and H. Weinfurter, *User-appropriate tire-modelling for vehicle dynamics in standard and limit situations*, Veh. Syst. Dyn. 38(2) (2002), pp. 103–125.
[3] W. Hirschberg, G. Rill, and H. Weinfurter, *Tire model TMeasy*, Veh. Syst. Dyn. 45(S1) (2007), pp. 101–119.
[4] G. Rill, *Simulation von Kraftfahrzeugen*, Vieweg-Verlag, Regensburg, Germany, 1994.
[5] A.J.C. Schmeitz and H.B. Pacejka, *A semi-empirical, three dimensional, tyre model for rolling over arbitrary road unevenesses*, Veh. Syst. Dyn. 41(suppl.) (2004), pp. 341–350.
[6] M. Gipser, *FTire a new fast tyre model for ride comfort situations*, International ADAMS User Conference, Berlin, Germany, 1999.
[7] J. Svendenius and M. Gäfvert, *A semi-empirical tyre model for combined slip forces*, Veh. Syst. Dyn. 44(2) (2006), pp. 189–208.
[8] G. Gim, Y. Choi, and S. Kim, *A semi-physical tyre model for a vehicle dynamics analysis of handling and braking*, Veh. Syst. Dyn. 45(S1) (2006), pp. 169–190.
[9] K. Guo and D. Lu, *UniTire: unified tyre model for vehicle dynamic simulation*, Veh. Syst. Dyn. 45(S1) (2007), pp. 79–99.

[10] Modelica Association, *Modelica Language Specification Version 3.0*, Linköping, Sweden, 2007; software available at http://www.modelica.org/documents/ModelicaSpec30.pdf.
[11] M. Otter, H. Elmquist, and S.E. Mattsson, *The new Modelica MultiBody Library*, Proceedings of the 3rd International Modelica Conference, Linköping, November 2003, pp. 11–18. Available at http://www.modelica.org/events/Conference2003/papers/h37_Otter_multibody.pdf.
[12] J. Andreasson, *Vehicle dynamics library*, Proceedings of the 3rd International Modelica Conference, 2003, Linköping, November 2003, pp. 11–18. Available at http://www.modelica.org/events/Conference2003/papers/h28_vehicle_Andreasson.pdf.
[13] M. Dempsey, M. Gäfvert, P. Harman, C. Kral, and M. Otter, *Coordinated automotive libraries for vehicle system modelling*, Proceedings of the 5th International Modelica Conference, Vienna, September 2006, pp. 33–41. Available at http://www.modelica.org/events/modelica2006/Proceedings/sessions/Session1b2.pdf.
[14] D.G. Wilson, *Bicycling Science*, MIT Press, 2004.
[15] G. Rill, *Wheel dynamics*, Proceedings of the DINAME 2007, Ilhabela, SP, Brazil, 2007. Available at http://homepages.fh-regensburg.de/ rig39165/paper/Wheel_Dynamics.pdf.
[16] A.B. Dynasim, *Dymola Users' Version 6.0*, Lund, Sweden, 2006; software available at http://www.dynasim.se.
[17] A.L. Schwab, J.P. Meijaard, and J.M. Papadopoulos, *Benchmark Results on the Linearized Equations of Motion of an Uncontrolled Bicycle*, KSME Internat. J. Mech. Sci. Technol. 19 (2005), pp. 292–304.
[18] K.J. Åström, R.E. Klein, and A. Lennartsson, *Bicycle dynamics and control: adapted bicycles for education and research*, IEEE Control Syst. Mag. 25(4) (2005), pp. 26–47.

Appendix 1. Notation of the most important symbols.

| Symbol | Modelica | Description | Type | Unit |
|---|---|---|---|---|
| *Positional states and their derivatives* | | | | |
| $\boldsymbol{C}_0$ | r_0 | Position of wheel frame | Real[3] | m |
| $\boldsymbol{v}_0$ | v_0 | Velocity of wheel frame | Real[3] | m/s |
| $\boldsymbol{\omega}$ | w | Angular velocity of wheel (body system) | Real[3] | rad/s |
| $\boldsymbol{\omega}_0$ | w_0 | Angular velocity of wheel (inertial system) | Real[3] | rad/s |
| $\boldsymbol{\omega}_{\text{roll}}$ | w_roll | Angular rolling velocity | Real[3] | rad/s |
| $\boldsymbol{\omega}_{\text{turn}}$ | w_turn | Angular turning velocity | Real[3] | rad/s |
| *Specification of mass and inertia* | | | | |
| $m$ | m | Mass of wheel | Real | kg |
| $\mathbf{I}$ | I | Inertia tensor of wheel | Real[3,3] | kg m$^2$ |
| *Fundamental geometry* | | | | |
| $r$ | r | Wheel radius | Real | m |
| width | width | Width of wheel | Real | m |
| $\boldsymbol{e}_{\text{n}}$ | eN | Unit normal vector of road plane | Real[3] | 1 |
| $\boldsymbol{e}_{\text{lat}}$ | eLat | Unit vector in road plane in lateral direction | Real[3] | 1 |
| $\boldsymbol{e}_{\text{long}}$ | eLong | Unit vector in road plane in longitudinal direction | Real[3] | 1 |
| $\boldsymbol{e}_{\text{axis}}$ | eAxis | Unit vector parallel to wheel axis | Real[3] | 1 |
| *Contact point and contact region* | | | | |
| $\boldsymbol{d}_{\text{W},0}$ | dCP_0 | Vector from wheel centre to contact point | Real[3] | m |
| $\boldsymbol{W}_0$ | rCP_0 | Position of contact point (on undeformed wheel) | Real[3] | m |
| $l_{\text{CR}}$ | LCR | Length of contact region | Real | m |
| $w_{\text{CR}}$ | WCR | Width of contact region | Real | m |
| $l_{\text{trail}}$ | LTrail | Length of trail | Real | m |
| $\text{sign}_{\text{trail}}$ | signTrail | Direction of trail | Real | 1 |
| camberDef$l$ | camberDefl | Lateral deflection due to the effect of camber | Real | m |
| maxCamberDef$l$ | maxCamberDefl | Maximal possible value for camberDefl | Real | m |
| *Slip velocities* | | | | |
| $v$Slip | vSlip | Total slip velocity | Real | m/s |
| $v\text{Slip}_{\text{lat}}$ | vSlipLat | Lateral slip velocity | Real | m/s |
| $v\text{Slip}_{\text{long}}$ | vSlipLong | Longitudinal slip velocity | Real | m/s |
| $v$CamberSlip | vCamberSlip | Lateral slip due to camber | Real | m/s |
| $v$Roll | vRoll | Roll velocity | Real | m/s |

*(continued)*

Appendix 1. Continued.

| Symbol | Modelica | Description | Type | Unit |
|---|---|---|---|---|
| *Forces and torques acting on the wheel* | | | | |
| $\boldsymbol{f}$ | f | Force acting at wheel centre | Real[3] | N |
| $\boldsymbol{f}_{\text{tyre},0}$ | fTire | Force acting on contact point | Real[3] | N |
| $f_{\text{n}}$ | fN | Component of $f_{\text{tyre},0}$ (normal direction) | Real | N |
| $f_{\text{lat}}$ | fLat | Component of $f_{\text{tyre},0}$ (lateral direction) | Real | N |
| $f_{\text{long}}$ | fLong | Component of $f_{\text{tyre},0}$ (longitudinal direction) | Real | N |
| $\boldsymbol{t}$ | t | Torque acting on centre | Real[3] | Nm |
| $\boldsymbol{t}_{\text{TB}}$ | tTB | Torque due to tyre trail | Real[3] | Nm |
| $\boldsymbol{t}_{\text{roll}}$ | tRoll | Torque due to roll resistance | Real[3] | Nm |
| $\boldsymbol{t}_{\text{turn}}$ | tTurn | Torque due to turning friction | Real[3] | Nm |
| *Specification of general friction characteristics* | | | | |
| $f_{\text{n},1}$ | fN1 | Normal load ($f_{\text{n},2} = 2f_{\text{n},1}$) | Real | N |
| $\mu_{\text{max,lat},1}$ | muMaxLat1 | Maximum friction coefficient at $f_{\text{n}} = f_{\text{n},1}$(lateral slip) | Real | 1 |
| $\mu_{\text{max,long},1}$ | muMaxLong1 | Maximum friction coefficient at $f_{\text{n}} = f_{\text{n},1}$(longitudinal slip) | Real | 1 |
| $\mu_{\text{min,lat},1}$ | muMinLat1 | Sliding friction coefficient at $f_{\text{n}} = f_{\text{n},1}$(lateral slip) | Real | 1 |
| $\mu_{\text{min,long},1}$ | muMinLong1 | Sliding friction coefficient at $f_{\text{n}} = f_{\text{n},1}$(longitudinal slip) | Real | 1 |
| $\mu_{\text{max,lat},2}$ | MuMaxLat2 | Maximum friction coefficient at $f_{\text{n}} = f_{\text{n},2}$(lateral slip) | Real | 1 |
| $\mu_{\text{max,long},2}$ | muMaxLong2 | Maximum friction coefficient at $f_{\text{n}} = f_{\text{n},2}$(longitudinal slip) | Real | 1 |
| $\mu_{\text{min,lat},2}$ | muMinLat2 | Sliding friction coefficient at $f_{\text{n}} = f_{\text{n},2}$(lateral slip) | Real | 1 |
| $\mu_{\text{min,long},2}$ | muMinLong2 | Sliding friction coefficient at $f_{\text{n}} = f_{\text{n},2}$(longitudinal slip) | Real | 1 |
| $v$Adhesion | vAdhesion | Region of adhesion | Real | m/s |
| $v$Slide | sSlide | Minimum velocity of sliding | Real | m/s |
| $s\text{Adhesion1}_{\text{lat}}$ | sAdhesionLat1 | Lateral slip at maximum force transmission if $f_{\text{n}} = f_{\text{n},1}$ | Real | 1 |
| $s\text{Adhesion1}_{\text{long}}$ | sAdhesionLong1 | Longitudinal slip at maximum force transmission if $f_{\text{n}} = f_{\text{n},1}$ | Real | 1 |
| $s\text{Slide1}_{\text{lat}}$ | sSlideLat1 | Lateral slip of sliding friction at $f_{\text{n}} = f_{\text{n},1}$ | Real | 1 |
| $s\text{Slide1}_{\text{long}}$ | sSlideLong1 | Longitudinal slip of sliding friction at $f_{\text{n}} = f_{\text{n},1}$ | Real | 1 |
| $s\text{Adhesion2}_{\text{lat}}$ | sAdhesionLat2 | Lateral slip at max force transmission if $f_{\text{n}} = f_{\text{n},2}$ | Real | 1 |
| $s\text{Adhesion2}_{\text{long}}$ | sAdhesionLong2 | Longitudinal slip at maximum force transmission if $f_{\text{n}} = f_{\text{n},2}$ | Real | 1 |
| $s\text{Slide2}_{\text{lat}}$ | sSlideLat2 | Lateral slip of sliding friction at $f_{\text{n}} = f_{\text{n},2}$ | Real | 1 |
| $s\text{Slide2}_{\text{long}}$ | sSlideLong2 | Longitudinal slip of sliding friction at $f_{\text{n}} = f_{\text{n},2}$ | Real | 1 |
| tol | tol | Softness of the softmax function | Real | 1 |
| $\mu_{\text{roll}}$ | muRoll | Friction coefficient of roll resistance | Real | 1 |
| $\mu_{\text{turn},1}$ | muTurn1 | Friction coefficient of turning resistance at $f_{\text{n}} = f_{\text{n},1}$ | Real | 1 |
| $\mu_{\text{turn},2}$ | muTurn2 | Friction coefficient of turning resistance at $f_{\text{n}} = f_{\text{n},2}$ | Real | 1 |
| $\text{gain}_{\text{Camber}}$ | gainCamber | Scaling of the camber slip | Real | 1/m |
| $\text{gain}_{\text{SA}}$ | gainSA | Scaling of self-alignment | Real | 1 |
| *Dynamic friction characteristics* | | | | |
| $\mu_{\text{max,lat}}$ | muMaxLat | Maximum friction coefficient (lateral slip) | Real | 1 |
| $\mu_{\text{max,long}}$ | muMaxLong | Maximum friction coefficient (longitudinal slip) | Real | 1 |
| $\mu_{\text{min,lat}}$ | muMinLat | Sliding friction coefficient (lateral slip) | Real | 1 |
| $\mu_{\text{min,long}}$ | muMinLong | Sliding friction coefficient (longitudinal slip) | Real | 1 |
| $s\text{Adhesion}_{\text{lat}}$ | sAdhesionLat | Lateral slip of maximum force transmission | Real | 1 |
| $s\text{Adhesion}_{\text{long}}$ | sAdhesionLong | Longitudinal slip of maximum force transmission | Real | 1 |
| $s\text{Slide}_{\text{lat}}$ | sSlideLat | Lateral slip of sliding friction | Real | 1 |
| $s\text{Slide}_{\text{long}}$ | sSlideLong | Longitudinal slip of sliding friction | Real | 1 |
| $\mu_{\text{max}}$ | muMax | Maximum friction coefficient in current direction | Real | 1 |
| $\mu_{\text{min}}$ | muMin | Sliding friction coefficient in current direction | Real | 1 |
| $s$Adhesion | sAdhesion | Slip of maximum force transmission | Real | 1 |
| $s$Slide | sSlide | Slip of sliding friction | Real | 1 |
| $v$AR | vAR | Point of maximum force transmission | Real | m/s |
| $v$SR | vSR | Point of full slippage | Real | m/s |
| $\mu_{\text{turn}}$ | muTurn | Friction coefficient of turning resistance | Real | 1 |

*(continued)*

Appendix 1. Continued.

| Symbol | Modelica | Description | Type | Unit |
|---|---|---|---|---|
| *Spring damping systems* | | | | |
| $s_{\mathrm{n}}$ | sN | Travel of virtual tyre spring (normal direction) | Real | m |
| $s_{\mathrm{lat}}$ | sLat | Travel of virtual tyre spring (lateral direction) | Real | m |
| $s_{\mathrm{long}}$ | sLong | Travel of virtual tyre spring (longitudinal direction) | Real | m |
| $c_{\mathrm{n}}$ | cN | Spring constant(normal direction) | Real | N/m |
| $c_{\mathrm{lat}}$ | cLat | Spring constant (lateral direction) | Real | N/m |
| $c_{\mathrm{long}}$ | cLong | Spring constant(longitudinal direction) | Real | N/m |
| $d_{\mathrm{n}}$ | dN | Damping constant(normal direction) | Real | Ns/m |
| $d_{\mathrm{lat}}$ | dLat | Damping constant (lateral direction) | Real | Ns/m |
| $d_{\mathrm{long}}$ | dLong | Damping constant(longitudinal direction) | Real | Ns/m |